Control Engineering Practice 18 (2010) 262–278

Contents lists available at ScienceDirect

Control Engineering Practice

journal homepage: www.elsevier.com/locate/conengprac

Embedded UAV model and LASER aiding techniques for inertial navigation systems

J.F. Vasconcelos *, C. Silvestre, P. Oliveira, B. Guerreiro

Institute for Systems and Robotics (ISR), Instituto Superior Técnico (IST), Av. Rovisco Pais, 1, Torre Norte, 8° Andar 1049-001, Lisbon, Portugal

ARTICLE INFO

Article history:
Received 15 February 2009
Accepted 12 November 2009
Available online 8 January 2010

Keywords:
Inertial navigation
Extended Kalman filters
Vehicle dynamics
Sensor fusion
Autonomous vehicles
Vertical takeoff and landing

ABSTRACT

This work proposes the integration of two aiding information sources to enhance the performance of inertial navigation systems (INS), for precise maneuvering of uninhabited air vehicles (UAVs). A new methodology is derived to exploit vehicle dynamics (VD) information by embeding the VD equations directly in an extended Kalman filter architecture. In this technique, the INS estimates are propagated simultaneously using the VD and the INS differential equations, allowing for the estimation of the INS errors. The proposed technique reduces the computational load associated with classical VD aiding, while retaining the same accuracy enhancements. A LASER range finder sensor is also integrated for precise landing and takeoff maneuvers. Simulation results for the nonlinear dynamics of a Vario X-Treme model-scale helicopter are presented, illustrating the contributions of the proposed aiding techniques for precise UAV navigation.

1. Introduction

The latest technological developments bring about uninhabited air vehicles (UAVs) as versatile, multipurpose platforms able to perform a wide variety of missions (Bijker & Steyn, 2008; Bryson & Sukkarieh, 2004; Koifman & Bar-Itzhack, 1999; Pflimlin, Binetti, Souères, Hamel, & Trouchet, 2009; Salazar-Cruz, Lozano, & Escareño, 2009). The vast scope of practical applications ranges from coastal surveillance, bridge monitoring, traffic watch, to domestic security, and search and rescue missions in extreme environments. Among the existing air vehicles, model-scale helicopters step forward as a challenging, high maneuverable platform with the ability to perform vertical takeoff and landing (VTOL), featuring complex, fast and unstable open-loop dynamics (Cunha & Silvestre, 2003; Kim & Tilbury, 2004; Mettler, 2002; Vissière, 2008).

To satisfy time enduring mission requirements, these vehicles are usually equipped with ultra light weight, low-cost navigation systems. The low-cost sensor units found in these systems are strongly affected by non-idealities, such as bias and noise, that degrade the accuracy of the estimates. To attain the required levels of performance and robustness, the sensor non-idealities are compensated for by merging aiding information sources into the navigation system. Although navigation system architectures aided by GPS measurements are commonly adopted, high accuracy requirements call for advanced filtering techniques that exploit precise aiding sensors as well as information about the UAV dynamics.

Vehicle model aiding can be adopted in nearly any application where the vehicle dynamics are known. It is of interest in indoor applications, urban scenarios, or hostile environments, where other aiding sensor can be inoperative or subject to jamming or distortion. Vehicle dynamics aiding is a software based solution that provides information about the UAV motion, and is combined with the inertial navigation estimates using filtering techniques. The integration of vehicle model with the inertial system kinematics allows for the compensation of inertial estimation errors, bearing performance improvements on state variables that are critical for precise maneuvering.

This paper discusses and proposes advanced aiding techniques for precise UAV position and attitude estimation using low-cost sensors. The navigation system architecture is based on merging a high accuracy inertial navigation system (INS) with the information obtained from the vehicle dynamics (VD), using an extended Kalman filter (EKF). A new method to integrate the vehicle dynamics in the navigation system is proposed, based on using the vehicle dynamics to propagate the INS state estimates, exploiting the redundancy of the information provided by the VD and by the high quality INS integration algorithms. Whereas classical methods integrate a full state vehicle simulator and require the estimation and compensation of the vehicle model errors, the new method integrates the VD directly in the EKF to

* Corresponding author. Tel.: +351 21 8418054; fax: +351 21 8418291.
E-mail addresses: jfvasconcelos@isr.ist.utl.pt, jfvasconcelos@gmail.com (J.F. Vasconcelos), cjs@isr.ist.utl.pt (C. Silvestre), pjcro@isr.ist.utl.pt (P. Oliveira). bguerreiro@isr.ist.utl.pt (B. Guerreiro).

0967-0661/$ - see front matter © 2009 Elsevier Ltd. All rights reserved.
doi:10.1016/j.conengprac.2009.11.004

estimate exclusively the INS errors. The proposed VD aiding method allows for the decoupling of the vehicle model differential equations, and selecting those that characterize the vehicle more accurately. Also, the computational cost associated with VD aiding is reduced due to the embedding of the vehicle model in the filter architecture, and to the use of inertial estimates in the computation of the vehicle dynamics.

The problem of precise distance-to-ground estimation is critical for aerial vehicles, namely during takeoff and landing maneuvers. A LASER range finder sensor implementation for takeoff and landing operations is detailed, enhancing the vertical channel position and velocity estimates. The proposed VD and LASER aiding techniques are demonstrated for a Vario X-Treme helicopter dynamic model, and the accuracy enhancements for takeoff, cruise and landing operations are evidenced in simulation. The computational savings of the proposed VD aiding with respect to the classical VD aiding technique are analyzed.

Classical GPS/INS architectures comprising inertial sensor biases estimation are found to hold only partial observability for a time-invariant configuration, as discussed in Goshen-Meskin and Bar-Itzhack (1992a, 1992b). The vehicle model aiding steps forward as an inexpensive, software based solution to overcome the lack of observability in the navigation system. Simple motion constraints have been successfully implemented in the past for land vehicle applications, by introducing the concept of virtual observations, see Bryson and Sukkarieh (2004), Ma, Sukkarieh, and Kim (2003), Dissanayake and Sukkarieh (2001). Non-holonomic constraints of wheeled vehicles, namely the inability to takeoff or perform lateral translation, are exploited in the navigation system by inputting zero valued virtual measurements of the body frame y- and z-axes velocity. Also, vehicle dynamics bandwidth information and frequency contents are successfully implemented to trace inertial motion and tackle bias misalignment errors in Vasconcelos, Oliveira, and Silvestre (2005).

Full state, complex aircraft dynamics have been adopted to enhance the observability of the navigation system in recent work presented in Bryson and Sukkarieh (2004) and Koifman and Bar-Itzhack (1999), and experimental results for a model-aided inertial navigation system for underwater vehicles can be found in Hegrenaes, Berglund, and Hallingstad (2008). In the architectures found in these references, the navigation system structure is composed by a VD block that plays the role of an extra INS unit. Given the vehicle model inputs, the vehicle model simulator computes angular and linear velocities that are compared to the INS estimates using the EKF algorithm. The EKF state model is augmented to dynamically estimate both the INS and the VD errors, improving the overall navigation system accuracy. Interestingly enough, the results presented in the literature (Bryson & Sukkarieh, 2004; Hegrenaes et al., 2008; Koifman & Bar-Itzhack, 1999) evidence that the velocity enhancements, brought about by VD aiding, can also reduce the drift of the position estimates, although position is not directly computed in the vehicle simulator (Bryson & Sukkarieh, 2004).

A drawback in complex vehicle dynamics lies in the modeling errors, over-parametrization of the model, and poor observability of the vehicle states, which degrades the filter performance, and that must be accounted for under the form of state model uncertainty and/or using weak constraints. A discussion about the impact of process model complexity on the improvement of the navigation system performance is presented in Julier and Durrant-Whyte (2003). In this reference, vehicle model aiding is shown to tackle state uncertainty and it is evidenced that small improvements in the VD model are more relevant to the performance enhancement than the choice of aiding sensor suites. Successful experimental validation of a model based observer for a Vario model-scale helicopter is found in Vissière, Bristeau, Martin, and Petit (2008) and Vissière (2008), evidencing that model aiding techniques can be adopted in these robotic platforms.

The proposed navigation system is based on a classical INS/EKF architecture, depicted in Fig. 1. The INS is a dead-reckoning algorithm that computes attitude, velocity and position based on the inertial sensor readings. High precision, multirate INS algorithms that account for high frequency attitude, velocity and position motions (denoted as coning, sculling and scrolling, respectively) are developed in Savage (1998a, 1998b) and Ignagni (1998). The inertial attitude, velocity and position estimates are affected by inertial sensor biases and noise, and filtering techniques such as the EKF are adopted to dynamically compensate for non-ideal sensor characteristics that otherwise yield unbounded INS errors. The EKF compares the aiding sensor and vehicle model information with the INS output, under the form of a measurement residual, and compensates for the inertial unit errors using a direct feedback configuration. Theory and application related to the EKF and INS algorithms can be found in Grewal, Weill, and Andrews (2007), Farrell and Barth (1999), Brown and Hwang (1997), Rogers (2003), Bar-Shalom, Li, and Kirubarajan (2001) and in references therein, where navigation strategies based on GPS/INS fusion are commonly adopted.

In the first architecture, shown in Fig. 1(a), the vehicle dynamics are computed by an external VD simulator based on the available thrusters input information. The distinct nature of the error sources and system dynamics allows the EKF to separate the INS errors from the VD errors and to perform their mutual updating in the compensation routines. Recalling the fundamentals of filtering and sensor fusion, the VD and INS ensemble is expected to yield better performance than any of the systems independently (Koifman & Bar-Itzhack, 1999). The accuracy of the INS is increased at the cost of integrating the VD model and states, augmenting the EKF states to compensate for the VD model errors, and using error compensation routines in the external vehicle model.

In the second architecture, that is the main contribution of the present paper, the VD information is merged in the EKF state model, as depicted in Fig. 1(b), using the INS states to compute the VD dynamics. In this setup, the inertial state estimates are fed to the INS and the VD equations, and the output of the VD algorithm is described as a function of the INS errors. The distinct VD and INS differential equations applied to the same inertial quantity enables the EKF to estimate and compensate for the inertial errors.

The proposed technique reduces the computational load associated with the classical VD aiding, and introduces some flexibility in the implementation of the vehicle model. Vehicle model differential equations are decoupled using the INS states in the VD computations, and it is possible to select only those dynamics that are more accurately modeled or that yield relevant information. For example, the classical aiding technique computes the attitude kinematics in the INS and in the vehicle simulator (Koifman & Bar-Itzhack, 1999), whereas the proposed aiding technique computes the attitude kinematics only in the INS. Also, in the proposed aiding technique, some of the vehicle differential equations are integrated numerically, while others are formulated directly as a filter measurement, which reduces the number of computations associated with the vehicle model aiding. The correction routines adopted in the classical vehicle model aiding, illustrated in Fig. 1(a), are not necessary in the proposed technique due to the embedding of the vehicle dynamics in the filter state model.

The derived vehicle aiding techniques are introduced and validated using a generic fully actuated rigid body simulator

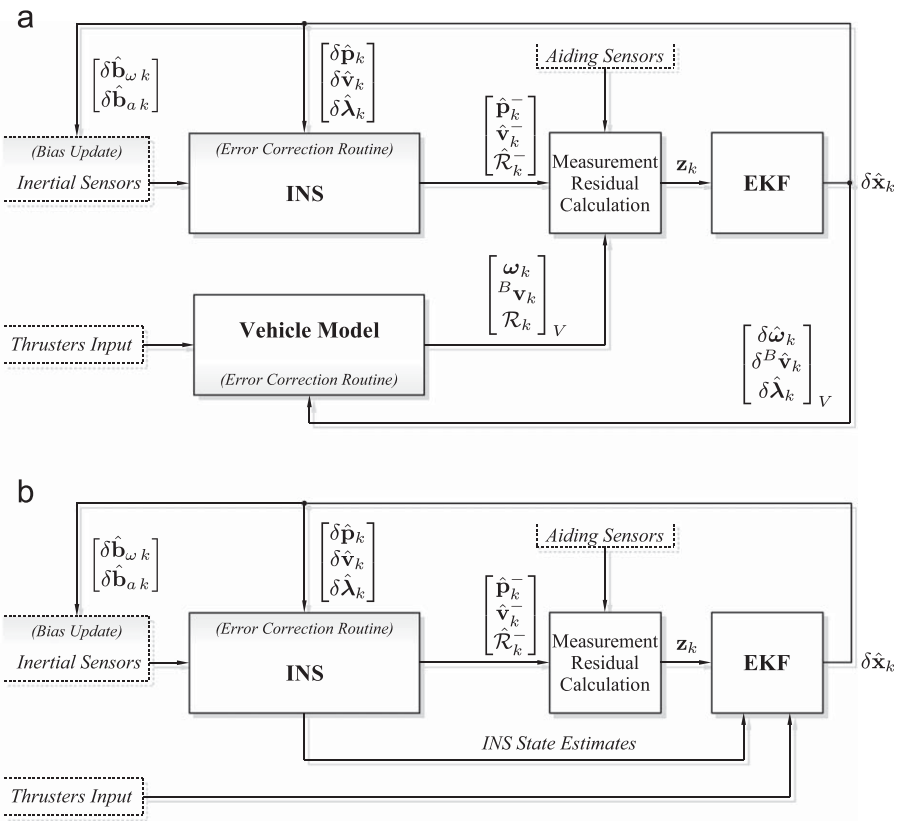

Fig. 1. Navigation system block diagram. (a) External vehicle dynamics. (b) Embedded vehicle dynamics.

example, and extended to a model-scale Vario X-Treme helicopter model simulator to demonstrate its application to realistic setups. A preliminary version of this work has been presented in Vasconcelos, Silvestre, and Oliveira (2006), and a validation in simulation of the proposed architecture for oceanic vehicles was presented in the subsequent publication (Morgado, Oliveira, Silvestre, & Vasconcelos, 2007).

This paper is organized as follows. Section 2 describes the inertial navigation system and the Kalman filtering algorithm adopted in this work. Section 3 presents the vehicle model aiding architectures, and the two methods to integrate the vehicle information in the navigation system are detailed. The dynamics of a fully actuated rigid body are described, and adopted to illustrate the VD aiding techniques. Section 4 characterizes the LASER sensor and describes the integration of the sensor information in the navigation system structure. Section 5 provides the implementation details. Namely, the state model of the EKF for each aiding technique, the discretization process and the error correction routines are detailed. Simulation results for the VD model and LASER range finder sensor are presented in Section 6. The classical VD is validated using a standard UAV trajectory, and tested with the Vario X-Treme helicopter model. The LASER aiding is studied by simulating a landing maneuver where the distance-to-ground is unknown. Concluding remarks are discussed in Section 7.

1.1. Nomenclature

The notation adopted is fairly standard. Column vectors and matrices are denoted, respectively, by lowercase and uppercase boldface type, e.g. $\mathbf{s}$ and $\mathbf{S}$. The transpose of a vector or matrix will be indicated by a prime, and trailing subscripts $\{x, y, z\}$ denote the vector components, $\mathbf{s} = [s_x \; s_y \; s_z]'$. Leading subscripts and superscripts identify the coordinate system of a quantity, e.g. ${}^{E}\mathbf{s}$ is represented in coordinate frame $\{E\}$, and ${}^{E}_{B}\mathbf{R}$ is a rotation matrix that transforms the vector representation ${}^{B}\mathbf{s}$ into ${}^{E}\mathbf{s}$ by means of the linear operation ${}^{E}\mathbf{s} = {}^{E}_{B}\mathbf{R}\,{}^{B}\mathbf{s}$. Position, velocity and acceleration are denoted, respectively, by $\mathbf{p}$, $\mathbf{v}$, and $\mathbf{a}$, and the angular velocity of the vehicle expressed in body coordinates is represented by $\boldsymbol{\omega}$. The measurement and the estimate of quantity $\mathbf{s}$ are denoted by $\mathbf{s}_r$ and $\hat{\mathbf{s}}$, respectively. The estimation error is defined as $\delta\mathbf{s} = \hat{\mathbf{s}} - \mathbf{s}$ unless otherwise noted, and $\|\mathbf{s}\|$ denotes the Frobenius norm. Discrete-time quantities are characterized by the time index k subscript. The $(n \times n)$ identity matrix is denoted by $\mathbf{I}_n$, and $(m \times n)$ zeros and ones matrices are, respectively, denoted by $\mathbf{0}_{m\times n}$ and $\mathbf{1}_{m\times n}$, where the subscript is omitted whenever clear from the context.

2. Navigation system structure

This section describes the adopted navigation system architecture that comprises a high accuracy, multirate INS integration algorithm, combined with advanced error compensation techniques based on Kalman filtering, as illustrated in Fig. 1. The INS algorithm integrates the rigid body kinematics differential equations from the output of inertial sensors, which allows for its use in any robotic platform regardless of the available position and attitude references, and irrespective of the vehicle dynamics. However, the INS position and attitude estimation errors will drift with time under the influence of accelerometer and rate gyro non-idealities such as noise, scaling factors, sensor misalignment and bias calibration errors, among others.

The EKF dynamically estimates the INS errors, by merging available aiding information such as GPS position measurements, attitude information contained in vector observations, and vehicle model dynamics, as illustrated in Fig. 1. The INS errors are then

compensated by modeling their first order description in state space form, comparing the aiding information with the INS estimates, and feeding back the errors estimate to the INS (direct-feedback configuration).

This section presents the main characteristics of the INS and EKF algorithms adopted in this work. The concept of multirate high accuracy inertial integration algorithm, the EKF state space formulation and the error compensation routines are introduced. The navigation system is presented concisely and for the sake of completeness, providing the necessary background for the LASER and the vehicle dynamics aiding techniques, for further details on the present architecture see Vasconcelos et al. (2005) and references therein.

2.1. Inertial navigation system

The INS performs attitude, velocity and position numerical integration from rate gyro and accelerometer triads data, rigidly mounted on the vehicle structure (strapdown configuration). For highly maneuverable vehicles, the INS numerical integration algorithm must properly address the fast dynamics of inertial sensors output, to avoid estimation errors buildup. The INS algorithm adopted in this paper is detailed on the tutorial work presented in Savage (1998a, 1998b). A multirate approach is adopted to account for angular position, linear velocity, and linear position high frequency motions, referred to as coning, sculling, and scrolling, respectively. In this framework, a high speed, low order algorithm computes dynamic angular rate/acceleration effects at a small sampling interval, and its output is periodically fed to a moderate-speed algorithm that computes attitude/velocity resorting to exact, closed-form equations.

The moderate-speed inertial algorithms represent attitude in rotation matrix form, and velocity and position are expressed in Earth frame coordinates. Simulation environments and case study trajectories to tune the algorithm's execution rates according to performance specifications are described in Savage (1998a, 1998b). A standard low-power consumption DSP based hardware architecture is found sufficient to run the algorithm at the highest accuracy repetition rates. Therefore, for a low cost architecture, high computational precision is obtained and the discrete-time integration errors are very small with respect to the other INS error sources such as inertial sensor bias and noise.

2.2. Extended Kalman filter

The inertial estimation errors are compensated for by merging the INS estimates with aiding information in the EKF algorithm (Brown & Hwang, 1997). The EKF error equations, based on perturbational rigid body kinematics, were brought to full detail in Britting (1971), and yield a first-order model of the INS estimation errors and sensor non-idealities. The nominal rigid body kinematics are given by

$$\dot{\mathbf{p}} = \mathbf{v}, \quad \dot{\mathbf{v}} = \mathcal{R}\,{}^{B}\mathbf{a}, \quad \dot{\mathcal{R}} = \mathcal{R}(\boldsymbol{\omega})_{\times}, \tag{1}$$

where the Earth and body frames are, respectively, denoted by $\{E\}$ and $\{B\}$, $\mathcal{R}$ is the shorthand notation for the rotation matrix ${}^{E}_{B}\mathbf{R}$, and $(\mathbf{s})_{\times}$ represents the skew symmetric matrix defined by the vector $\mathbf{s}\in\mathbb{R}^3$ such that $(\mathbf{s})_{\times}\mathbf{r} = \mathbf{s}\times\mathbf{r}$, $\mathbf{r}\in\mathbb{R}^3$. The angular velocity and the acceleration of the body are measured, respectively, by the accelerometer and rate gyro triads, corrupted by noise and bias as follows:

$$\boldsymbol{\omega}_r = \boldsymbol{\omega} + \mathbf{b}_{\omega} + \mathbf{n}_{\omega} - \hat{\mathbf{b}}_{\omega}, \tag{2a}$$

$$\mathbf{a}_r = {}^{B}\mathbf{a} - {}^{B}\mathbf{g} + \mathbf{b}_a + \mathbf{n}_a - \hat{\mathbf{b}}_a, \tag{2b}$$

where $\mathbf{g}$ represents Earth's gravitational field, the sensor biases are denoted by $\mathbf{b}_a$ and $\mathbf{b}_{\omega}$, and $\mathbf{n}_a \sim \mathcal{N}(\mathbf{0}, \Xi_a)$, $\mathbf{n}_{\omega} \sim \mathcal{N}(\mathbf{0}, \Xi_{\omega})$ are Gaussian white noise processes. The inertial sensor biases are modeled as random walk processes,

$$\dot{\mathbf{b}}_{\omega} = \mathbf{n}_{b_{\omega}}, \quad \dot{\mathbf{b}}_a = \mathbf{n}_{b_a},$$

where $\mathbf{n}_{b_{\omega}} \sim \mathcal{N}(\mathbf{0}, \Xi_{b_{\omega}})$ and $\mathbf{n}_{b_a} \sim \mathcal{N}(\mathbf{0}, \Xi_{b_a})$ are Gaussian white noise processes.

The rigid body coordinates are estimated using the available inertial sensor information

$$\dot{\hat{\mathbf{p}}} = \hat{\mathbf{v}}, \quad \dot{\hat{\mathbf{v}}} = \hat{\mathcal{R}}\mathbf{a}_r + {}^{E}\mathbf{g}, \quad \dot{\hat{\mathcal{R}}} = \hat{\mathcal{R}}(\boldsymbol{\omega}_r)_{\times}, \quad \dot{\hat{\mathbf{b}}}_a = \mathbf{0}, \quad \dot{\hat{\mathbf{b}}}_{\omega} = \mathbf{0}. \tag{3}$$

The position, velocity and bias estimation errors are defined by the difference between the estimated and nominal quantities,

$$\delta\mathbf{p} \coloneqq \hat{\mathbf{p}} - \mathbf{p}, \quad \delta\mathbf{v} \coloneqq \hat{\mathbf{v}} - \mathbf{v}, \quad \delta\mathbf{b}_a \coloneqq \hat{\mathbf{b}}_a - \mathbf{b}_a, \quad \delta\mathbf{b}_{\omega} \coloneqq \hat{\mathbf{b}}_{\omega} - \mathbf{b}_{\omega},$$

and the attitude error, denoted as $\delta\boldsymbol{\lambda}$, is parametrized by an unconstrained rotation vector representation in Earth coordinates, which can be assumed locally linear and non-singular, for details and equivalent attitude parametrizations, see Markley (2003) and Pittelkau (2003). Define the rotation error matrix as $\mathbf{R}(\delta\boldsymbol{\lambda}) \coloneqq \hat{\mathcal{R}}\mathcal{R}'$, the attitude error rotation vector $\delta\boldsymbol{\lambda}$ is described by the first order approximation

$$\mathbf{R}(\delta\boldsymbol{\lambda}) \simeq \mathbf{I}_3 + (\delta\boldsymbol{\lambda})_{\times} \Rightarrow (\delta\boldsymbol{\lambda})_{\times} \simeq \hat{\mathcal{R}}\mathcal{R}' - \mathbf{I}_3, \tag{4}$$

that is valid for "small-angle" attitude errors (Britting, 1971).

Combining (1)–(3), the attitude, velocity, and position error kinematics are obtained by retaining the first-order terms of Taylor's series expansions or by using perturbation algebraic techniques (Britting, 1971), producing

$$\delta\dot{\mathbf{p}} = \delta\mathbf{v}, \quad \delta\dot{\mathbf{v}} = \hat{\mathcal{R}}(\mathbf{a}_r - \mathbf{a}_{\mathrm{SF}}) - (\hat{\mathcal{R}}\mathbf{a}_r)_{\times}\delta\boldsymbol{\lambda}, \quad \delta\dot{\boldsymbol{\lambda}} = \mathcal{R}(\boldsymbol{\omega}_r - \boldsymbol{\omega}), \tag{5a}$$

$$\delta\dot{\mathbf{b}}_a = -\mathbf{n}_{b_a}, \quad \delta\dot{\mathbf{b}}_{\omega} = -\mathbf{n}_{b_{\omega}}, \tag{5b}$$

where $\mathbf{a}_{\mathrm{SF}} = {}^{B}\mathbf{a} - {}^{B}\mathbf{g}$ is the specific force, defined as the nominal reading of an accelerometer. The terms $(\boldsymbol{\omega}_r - \boldsymbol{\omega})$ and $(\mathbf{a}_r - \mathbf{a}_{\mathrm{SF}})$ represent, respectively, the non-idealities of the accelerometer and rate gyro readings, expressed in (2), and are described by

$$(\boldsymbol{\omega}_r - \boldsymbol{\omega}) = -\delta\mathbf{b}_{\omega} + \mathbf{n}_{\omega}, \quad (\mathbf{a}_r - \mathbf{a}_{\mathrm{SF}}) = -\delta\mathbf{b}_a + \mathbf{n}_a. \tag{6}$$

Combining (5) and (6), the error state space model is

$$\delta\dot{\mathbf{p}} = \delta\mathbf{v}, \quad \delta\dot{\mathbf{v}} = -\hat{\mathcal{R}}\delta\mathbf{b}_a - (\hat{\mathcal{R}}\mathbf{a}_r)_{\times}\delta\boldsymbol{\lambda} + \hat{\mathcal{R}}\mathbf{n}_a, \tag{7a}$$

$$\delta\dot{\boldsymbol{\lambda}} = -\hat{\mathcal{R}}\delta\mathbf{b}_{\omega} + \hat{\mathcal{R}}\mathbf{n}_{\omega}, \quad \delta\dot{\mathbf{b}}_a = -\mathbf{n}_{b_a}, \quad \delta\dot{\mathbf{b}}_{\omega} = -\mathbf{n}_{b_{\omega}}. \tag{7b}$$

The Kalman filter adopted in this work is based on the concept of Multiplicative EKF (Lefferts, Markley, & Shuster, 1982; Markley, 2003). In this architecture, global position and attitude parametrizations are adopted in INS algorithm, while local representations of the estimation errors are modeled in the EKF. In particular, the adopted attitude error parametrization is locally linear and hence can be integrated in the EKF algorithm without violating the constraints found in global attitude parametrizations, such as rotation matrices and quaternions. As illustrated in Fig. 1, the EKF estimates the INS error vector $\delta\mathbf{x} = [\delta\mathbf{p}'\ \delta\mathbf{v}'\ \delta\boldsymbol{\lambda}'\ \delta\mathbf{b}_a'\ \delta\mathbf{b}_{\omega}']'$, that is then fed back and stored in the global quantity $\mathbf{x}_{\mathrm{INS}} = (\mathbf{p}, \mathbf{v}, \mathcal{R}, \mathbf{b}_a, \mathbf{b}_{\omega})$, and reset in the filter. This process preserves the small error assumption underlying the linearized model (7), and its validity is demonstrated in Markley (2003), where it is also evidenced that the estimation error covariance is unaffected when $\delta\mathbf{x}$ is incorporated in $\mathbf{x}_{\mathrm{INS}}$.

3. Vehicle model aiding

In this section, the vehicle model aiding techniques are detailed. The classical and the new techniques to exploit the vehicle dynamics in the navigation system are presented and discussed. Without any loss of generality, the VD aiding technique proposed in this paper is illustrated using the dynamics of a 6-DOF rigid body polyhedron with uniform mass density and fully actuated. Afterward, the proposed technique is applied to a Vario X-Treme helicopter dynamic model, to demonstrate that the VD aiding technique is valid for realistic robotic platforms. Note that the Vario X-Treme helicopter is a challenging platform due to the complex dynamics of the vehicle, detailed in Appendix A, that are highly nonlinear and coupled.

3.1. Rigid body dynamics

The body coordinate frame origin, denoted $\mathbf{p}_{Borg}$, is located at the body's center of mass and geometric center. The axes of the body frame define a plane of symmetry for the mass distribution of the body, so the resulting body inertia tensor, denoted $\mathbf{I}_B$, is described by the principal moments of inertia (Craig, 1989), yielding

$$\mathbf{I}_B = \frac{m}{12}\begin{bmatrix} h^2+l^2 & 0 & 0 \\ 0 & w^2+h^2 & 0 \\ 0 & 0 & l^2+w^2 \end{bmatrix},$$

where m is the body mass and (l,w,h) represent the polyhedron length, width and height, respectively. The rigid body is subject to the thrusters force and momentum, denoted by $\mathbf{f}_{\text{th}}$ and $\mathbf{n}_{\text{th}}$, respectively, and to viscous linear and angular damping, denoted by $\mathbf{f}_d$ and $\mathbf{n}_d$, respectively, described by ${}^B\mathbf{f}_{\text{th}} = \sum_i {}^B\mathbf{f}_i$, ${}^B\mathbf{n}_{\text{th}} = \sum_i {}^B\mathbf{p}_{\text{th}\,i} \times {}^B\mathbf{f}_i$, ${}^B\mathbf{f}_d = -K_{\text{lin}}{}^B\mathbf{v}$, ${}^B\mathbf{n}_d = -K_{\text{ang}}\boldsymbol{\omega}$, where $i = 1,\ldots,6$ is the index of the thruster applying force $\mathbf{f}_i$ to the body, ${}^B\mathbf{p}_{\text{th}\,i}$ are the thrusters' coordinates in body frame, and K_{lin} and K_{ang} are, respectively, the linear and the angular damping coefficients.

Applying the Newton and Euler equations to determine body's translation and rotation with respect to the inertial frame, the body dynamics are expressed by the nonlinear state space model

$$\dot{\boldsymbol{\omega}}_V \coloneqq f_\omega(\boldsymbol{\omega}_V, \mathbf{n}_{\text{th}}) = -\mathbf{I}_B^{-1}((\boldsymbol{\omega}_V)_\times \mathbf{I}_B\boldsymbol{\omega}_V + K_{\text{ang}}\boldsymbol{\omega}_V) + \mathbf{I}_B^{-1}\mathbf{n}_{\text{th}}, \tag{8a}$$

$$\begin{aligned}{}^B\dot{\mathbf{v}}_V &\coloneqq f_v(\boldsymbol{\omega}_V, {}^B\mathbf{v}_V, \mathbf{f}_{\text{th}}) \\ &= -\mathbf{M}_T^{-1}((\boldsymbol{\omega}_V)_\times \mathbf{M}_T{}^B\mathbf{v}_V + K_{\text{lin}}{}^B\mathbf{v}_V) + \mathbf{M}_T^{-1}\mathbf{f}_{\text{th}} + \mathcal{R}_V'{}^E\mathbf{g},\end{aligned} \tag{8b}$$

$$\dot{\mathcal{R}}_V \coloneqq f_{\mathcal{R}}(\boldsymbol{\omega}_V, \mathcal{R}_V) = \mathcal{R}_V(\boldsymbol{\omega}_V)_\times, \tag{8c}$$

where the body and center of mass coordinate frames are defined with the same orientation and position, so that the body frame attitude dynamics (8a) do not depend on the linear velocity. To avoid ambiguity in the adopted notation, ${}^B\dot{\mathbf{v}}$ denotes $\mathrm{d}^B\mathbf{v}/\mathrm{dt}$, whereas ${}^B(\mathrm{d}\mathbf{v}/\mathrm{dt})$ is denoted by ${}^B(\dot{\mathbf{v}})$.

The simple rigid body dynamics (8) allow for physical intuition on the contribution of the vehicle model to the inertial states error compensation. The V subscript for the angular velocity and body linear velocity (8) is adopted to emphasize that these quantities are computed using the vehicle dynamics, given that some are also computed by the INS, using distinct integration algorithms and inputs.

The position is not computed in the vehicle model aiding technique because the position is decoupled from the other vehicle states in (8), and the vehicle position kinematics are identical to those of the INS. Although the vehicle attitude kinematics are also identical to those of the INS, the attitude is coupled with the other states of the vehicle and hence is explicitly modeled in (8). Interestingly enough, (8c) is computed in the external vehicle model aiding technique, replicating the INS computations, while the embedded vehicle model aiding technique exploits the INS attitude computations directly, as shown in the ensuing.

3.2. External vehicle model aiding

In the classical VD aiding, described in Koifman and Bar-Itzhack (1999) and Bryson and Sukkarieh (2004) and depicted in Fig. 1(a), the vehicle state estimates are computed by a standalone vehicle simulator, using the thrusters input information. The full state vehicle model algorithm computes attitude and velocity estimates that are compared to the INS output, under the form of measurement residuals. The EKF state model is augmented to estimate and compensate for the VD block errors, using model specific error compensation routines.

The VD block error dynamics are formulated using the technique adopted to describe the INS error dynamics in Section 2.2. These are obtained by applying a perturbational analysis to the nominal dynamics (8). Let $\hat{\mathbf{x}}_V = (\hat{\boldsymbol{\omega}}_V, {}^B\hat{\mathbf{v}}_V, \hat{\mathcal{R}}_V)$ denote the states estimated by the vehicle model simulator, the vehicle model error dynamics are described by the first order terms of the Taylor series expansion

$$\dot{\hat{\boldsymbol{\omega}}}_V = f_\omega(\hat{\boldsymbol{\omega}}_V, \hat{\mathbf{n}}_{\text{th}}) \Rightarrow \delta\dot{\boldsymbol{\omega}}_V \approx \left.\frac{\partial f_\omega}{\partial \boldsymbol{\omega}}\right|_{\mathbf{x}_V} \delta\boldsymbol{\omega}_V + \left.\frac{\partial f_\omega}{\partial \mathbf{n}_{\text{th}}}\right|_{\mathbf{x}_V} \delta\mathbf{n}_{\text{th}}, \tag{9a}$$

$$\begin{aligned}{}^B\dot{\hat{\mathbf{v}}}_V &= f_v(\hat{\boldsymbol{\omega}}_V, {}^B\hat{\mathbf{v}}_V, \hat{\mathcal{R}}_V, \hat{\mathbf{f}}_{\text{th}}) \\ &\Rightarrow \delta{}^B\dot{\mathbf{v}}_V \approx \left.\frac{\partial f_v}{\partial \boldsymbol{\omega}_V}\right|_{\mathbf{x}_V} \delta\boldsymbol{\omega}_V + \left.\frac{\partial f_v}{\partial {}^B\mathbf{v}_V}\right|_{\mathbf{x}_V} \delta{}^B\mathbf{v}_V \\ &\quad + \left.\frac{\partial f_v}{\partial \delta\boldsymbol{\lambda}}\right|_{\mathbf{x}_V} \delta\boldsymbol{\lambda}_V + \left.\frac{\partial f_v}{\partial \mathbf{f}_{\text{th}}}\right|_{\mathbf{x}_V} \delta\mathbf{f}_{\text{th}},\end{aligned} \tag{9b}$$

$$\dot{\hat{\mathcal{R}}}_V = f_{\mathcal{R}}(\hat{\boldsymbol{\omega}}_V, \hat{\mathcal{R}}_V) \Rightarrow \dot{\delta\boldsymbol{\lambda}}_V = \mathcal{R}_V\delta\boldsymbol{\omega}_V, \tag{9c}$$

where $\delta\boldsymbol{\omega}_V = \hat{\boldsymbol{\omega}}_V - \boldsymbol{\omega}$, $\delta{}^B\mathbf{v}_V = {}^B\hat{\mathbf{v}}_V - {}^B\mathbf{v}$, $\delta\mathbf{n}_{\text{th}} = \hat{\mathbf{n}}_{\text{th}} - \mathbf{n}_{\text{th}}$, $\delta\mathbf{f}_{\text{th}} = \hat{\mathbf{f}}_{\text{th}} - \mathbf{f}_{\text{th}}$, and the Jacobians are given by

$$\left.\frac{\partial f_\omega}{\partial \boldsymbol{\omega}}\right|_{\mathbf{x}_V} = \mathbf{I}_B^{-1}((\mathbf{I}_B\boldsymbol{\omega}_V)_\times - (\boldsymbol{\omega}_V)_\times\mathbf{I}_B - \mathbf{I}_3K_{\text{ang}}), \quad \left.\frac{\partial f_\omega}{\partial \mathbf{n}_{\text{th}}}\right|_{\mathbf{x}_V} = \mathbf{I}_B^{-1}, \tag{10a}$$

$$\left.\frac{\partial f_v}{\partial \boldsymbol{\omega}}\right|_{\mathbf{x}_V} = \mathbf{M}_T^{-1}(\mathbf{M}_T{}^B\mathbf{v}_V)_\times, \quad \left.\frac{\partial f_v}{\partial \mathbf{f}_{\text{th}}}\right|_{\mathbf{x}_V} = \mathbf{M}_T^{-1}, \tag{10b}$$

$$\left.\frac{\partial f_v}{\partial {}^B\mathbf{v}}\right|_{\mathbf{x}_V} = \mathbf{M}_T^{-1}(-(\boldsymbol{\omega}_V)_\times\mathbf{M}_T - \mathbf{I}_3K_{\text{lin}}), \quad \left.\frac{\partial f_v}{\partial \delta\boldsymbol{\lambda}}\right|_{\mathbf{x}_V} = \mathcal{R}_V'({}^E\mathbf{g})_\times. \tag{10c}$$

The first order model (9) can also be obtained by perturbational analysis of the dynamics (8). The rotation matrix kinematics (8c) are identical to the inertial rigid body kinematics expressed in (1), and consequently do not yield new information to the system. However, the computation of $\mathcal{R}_V$ is necessary for the vehicle dynamics simulator (8), and the associated error dynamics (9c), which are identical to the INS attitude error (5), must be compensated for.

The INS and VD state estimates are compared under the form of measurement residuals, obtained by the perturbational method adopted in Britting (1971), and described by

$$\begin{aligned}\mathbf{z}_\omega &\coloneqq \hat{\boldsymbol{\omega}} - \hat{\boldsymbol{\omega}}_V = \boldsymbol{\omega} + \delta\boldsymbol{\omega} - (\boldsymbol{\omega} + \delta\boldsymbol{\omega}_V) = \delta\boldsymbol{\omega} - \delta\boldsymbol{\omega}_V \\ &= -\delta\mathbf{b}_\omega - \delta\boldsymbol{\omega}_V + \mathbf{n}_\omega,\end{aligned} \tag{11a}$$

$$\begin{aligned}\mathbf{z}_v &\coloneqq \hat{\mathcal{R}}'\hat{\mathbf{v}} - {}^B\hat{\mathbf{v}}_V = \hat{\mathcal{R}}'\mathbf{v} - ({}^B\mathbf{v} + \delta{}^B\mathbf{v}_V) = (\hat{\mathcal{R}}' - \mathcal{R}')\mathbf{v} + \mathcal{R}'\delta\mathbf{v} - \delta{}^B\mathbf{v}_V \\ &= -\hat{\mathcal{R}}'(\boldsymbol{\lambda})_\times\mathbf{v} + \mathcal{R}'\delta\mathbf{v} - \delta{}^B\mathbf{v}_V \approx \mathcal{R}'\delta\mathbf{v} + \mathcal{R}'(\mathbf{v})_\times\delta\boldsymbol{\lambda} - \delta{}^B\mathbf{v}_V,\end{aligned} \tag{11b}$$

$$\mathbf{z}_{\mathcal{R}} \coloneqq \hat{\mathcal{R}}\hat{\mathcal{R}}_V' - \mathbf{I} \approx [\mathbf{I} + (\delta\boldsymbol{\lambda})_\times]\mathcal{R}\mathcal{R}'[\mathbf{I} - (\delta\boldsymbol{\lambda}_V)_\times] - \mathbf{I} \approx \delta\boldsymbol{\lambda} - \delta\boldsymbol{\lambda}_V, \tag{11c}$$

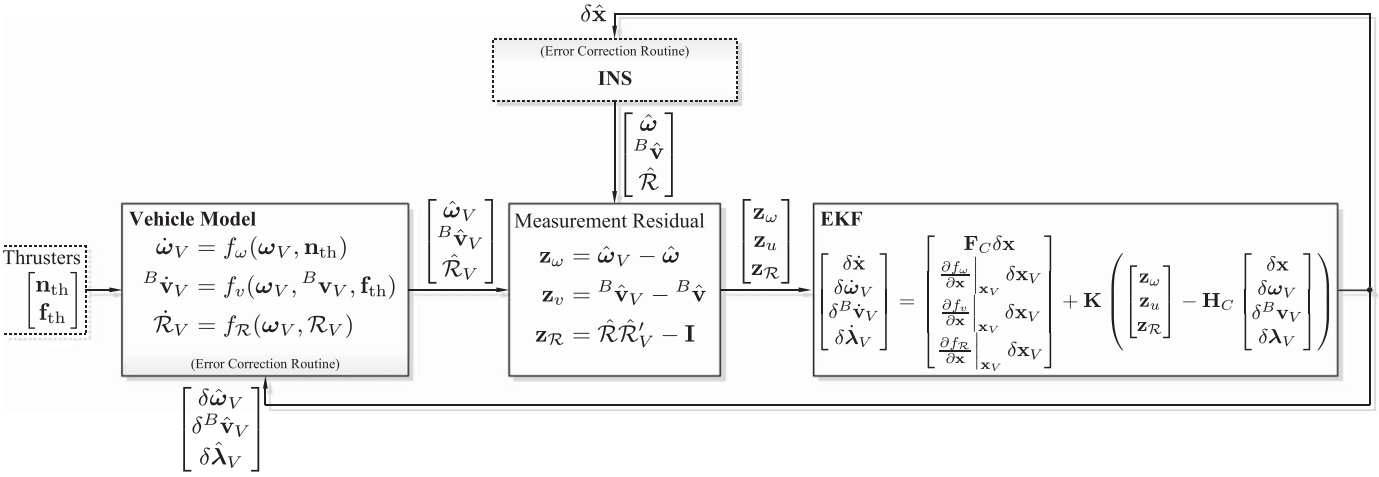

Fig. 2. External vehicle model aiding for the 6-DOF rigid body polyhedron.

where $\hat{\boldsymbol{\omega}}$ is the angular velocity estimate given by the INS, i.e. $\hat{\boldsymbol{\omega}} = \boldsymbol{\omega}_r$.

The external VD aiding technique is detailed in Fig. 2. The vehicle model equations (8) are computed by a variable-step Runge–Kutta differential equation solver, using the thrusters force $\mathbf{f}_{th}$ and momentum $\mathbf{n}_{th}$ information. The vehicle state errors and covariances are propagated by the EKF using the first order model (9) and assuming that the thrusters input is known from the control system, $\delta\mathbf{n}_{th} = \delta\mathbf{f}_{th} = \mathbf{0}$. In experimental applications the inputs of the vehicle model may not be accurately known, and $\delta\mathbf{n}_{th}$, $\delta\mathbf{f}_{th}$ may be modeled as small stochastic uncertainties to increase the navigation system robustness.

The INS and VD errors are estimated by processing the measurement residuals (11) in the EKF algorithm. Similar to the storage technique used for the INS error compensation, described in Section 2.2, the estimated VD errors $\delta\mathbf{x}_V = [\delta\boldsymbol{\omega}_V' \;\; \delta^B\mathbf{v}_V' \;\; \delta\boldsymbol{\lambda}_V']'$ are transferred to the external VD block and used to update the state $\mathbf{x}_V = (\boldsymbol{\omega}_V, {}^B\mathbf{v}_V, \mathcal{R}_V)$. This method preserves the small error conditions of the first order model (8), however, it requires the implementation of error compensation routines in the vehicle model.

3.3. Embedded vehicle model aiding

The vehicle model aiding enhances the accuracy of the navigation system by providing specific information about the robotic platform, e.g. its linear and angular velocity dynamics, (8a) and (8b), respectively. In the classical technique described in the last section, the attitude kinematics (8c) are computed simultaneously in the INS and in the self-contained vehicle simulator, and vehicle model errors compensation routines must be implemented, as illustrated in Fig. 1. The necessity of these auxiliary computational routines, and of distinct vehicle states that partially replicate those found in the INS, motivates an alternative vehicle model integration method, that embeds the VD equations directly in the EKF state model as shown in Fig. 1(b).

The embedded VD aiding concept is based on using the vehicle dynamics to propagate the INS estimates. Due to the presence of inertial estimation errors, the results obtained by solving the vehicle dynamics using the inertial estimates is different from the INS state estimate derivatives, that is $\dot{\hat{\boldsymbol{\omega}}} \neq f_\omega(\hat{\boldsymbol{\omega}}, \hat{\mathbf{n}}_{th})$, $\dot{\hat{\mathbf{v}}} \neq f_v(\hat{\boldsymbol{\omega}}, {}^B\hat{\mathbf{v}}, \hat{\mathcal{R}}, \hat{\mathbf{f}}_{th})$. To exploit the distinct, but compatible models enclosed in the VD and INS computations, the VD results are described as a function of the INS errors, enabling the EKF to estimate and compensate for the inertial errors. Interestingly enough, the proposed embedded VD aiding reduces the computational cost associated with vehicle aiding, while bearing the same estimation error accuracy.

With a slight abuse of notation, let $\hat{\mathbf{x}} = (\hat{\boldsymbol{\omega}}, \hat{\mathbf{v}}, \hat{\mathcal{R}}, \hat{\mathbf{b}}_a, \hat{\mathbf{b}}_\omega)$ denote the INS state estimates. In the embedded VD methodology, nominal vehicle dynamics (8) are linearized about the INS state estimates, using the first order terms of the Taylor series expansion, yielding

$$\dot{\boldsymbol{\omega}} = f_\omega(\boldsymbol{\omega}, \mathbf{n}_{th}) \approx f_\omega(\hat{\boldsymbol{\omega}}, \hat{\mathbf{n}}_{th}) + \left.\frac{\partial f_\omega}{\partial \boldsymbol{\omega}}\right|_{\hat{\mathbf{x}}} (\boldsymbol{\omega} - \hat{\boldsymbol{\omega}}) + \left.\frac{\partial f_\omega}{\partial \mathbf{n}_{th}}\right|_{\hat{\mathbf{x}}} (\mathbf{n}_{th} - \hat{\mathbf{n}}_{th}),$$

$$\begin{aligned} {}^B\dot{\mathbf{v}} = f_v(\boldsymbol{\omega}, {}^B\mathbf{v}, \mathcal{R}, \mathbf{f}_{th}) &\approx f_v(\hat{\boldsymbol{\omega}}, {}^B\hat{\mathbf{v}}, \hat{\mathcal{R}}, \hat{\mathbf{f}}_{th}) + \left.\frac{\partial f_v}{\partial \boldsymbol{\omega}}\right|_{\hat{\mathbf{x}}} (\boldsymbol{\omega} - \hat{\boldsymbol{\omega}}) \\ &+ \left.\frac{\partial f_v}{\partial {}^B\mathbf{v}}\right|_{\hat{\mathbf{x}}} ({}^B\mathbf{v} - {}^B\hat{\mathbf{v}}) + \left.\frac{\partial f_v}{\partial \delta\boldsymbol{\lambda}}\right|_{\hat{\mathbf{x}}} \delta\boldsymbol{\lambda} + \left.\frac{\partial f_v}{\partial \mathbf{f}_{th}}\right|_{\hat{\mathbf{x}}} (\mathbf{f}_{th} - \hat{\mathbf{f}}_{th}). \end{aligned}$$

Given the definition of the INS estimation error, the nominal angular and linear velocities are expressed as a function of the INS states and estimation errors by

$$\begin{aligned} \dot{\boldsymbol{\omega}} &\approx f_\omega(\hat{\boldsymbol{\omega}}, \hat{\mathbf{n}}_{th}) - \left.\frac{\partial f_\omega}{\partial \boldsymbol{\omega}}\right|_{\hat{\mathbf{x}}} \delta\boldsymbol{\omega} - \left.\frac{\partial f_\omega}{\partial \mathbf{n}_{th}}\right|_{\hat{\mathbf{x}}} \delta\mathbf{n}_{th} \\ &= f_\omega(\hat{\boldsymbol{\omega}}, \hat{\mathbf{n}}_{th}) + \left.\frac{\partial f_\omega}{\partial \boldsymbol{\omega}}\right|_{\hat{\mathbf{x}}} \delta\mathbf{b}_\omega - \left.\frac{\partial f_\omega}{\partial \boldsymbol{\omega}}\right|_{\hat{\mathbf{x}}} \mathbf{n}_\omega - \left.\frac{\partial f_\omega}{\partial \mathbf{n}_{th}}\right|_{\hat{\mathbf{x}}} \delta\mathbf{n}_{th}, \end{aligned} \tag{12a}$$

$$\begin{aligned} {}^B\dot{\mathbf{v}} &\approx f_v(\hat{\boldsymbol{\omega}}, {}^B\hat{\mathbf{v}}, \hat{\mathcal{R}}, \hat{\mathbf{f}}_{th}) - \left.\frac{\partial f_v}{\partial \boldsymbol{\omega}}\right|_{\hat{\mathbf{x}}} \delta\boldsymbol{\omega} - \left.\frac{\partial f_v}{\partial {}^B\mathbf{v}}\right|_{\hat{\mathbf{x}}} \delta^B\mathbf{v} - \left.\frac{\partial f_v}{\partial \delta\boldsymbol{\lambda}}\right|_{\hat{\mathbf{x}}} \delta\boldsymbol{\lambda} \\ &\quad - \left.\frac{\partial f_v}{\partial \mathbf{n}_{th}}\right|_{\hat{\mathbf{x}}} \delta\mathbf{n}_{th} - \left.\frac{\partial f_v}{\partial \mathbf{f}_{th}}\right|_{\hat{\mathbf{x}}} \delta\mathbf{f}_{th} \\ &= f_v(\hat{\boldsymbol{\omega}}, {}^B\hat{\mathbf{v}}, \hat{\mathcal{R}}, \hat{\mathbf{f}}_{th}) - \left.\frac{\partial f_v}{\partial {}^B\mathbf{v}}\right|_{\hat{\mathbf{x}}} \mathcal{R}'\delta\mathbf{v} - \left(\left.\frac{\partial f_v}{\partial \delta\boldsymbol{\lambda}}\right|_{\hat{\mathbf{x}}} + \left.\frac{\partial f_v}{\partial \mathbf{v}}\right|_{\hat{\mathbf{x}}} \mathcal{R}'(\mathbf{v})_\times\right)\delta\boldsymbol{\lambda} \\ &\quad + \left.\frac{\partial f_v}{\partial \boldsymbol{\omega}}\right|_{\hat{\mathbf{x}}} \delta\mathbf{b}_\omega - \left.\frac{\partial f_v}{\partial \boldsymbol{\omega}}\right|_{\hat{\mathbf{x}}} \mathbf{n}_\omega - \left.\frac{\partial f_v}{\partial \mathbf{n}_{th}}\right|_{\hat{\mathbf{x}}} \delta\mathbf{n}_{th} - \left.\frac{\partial f_v}{\partial \mathbf{f}_{th}}\right|_{\hat{\mathbf{x}}} \delta\mathbf{f}_{th}, \end{aligned} \tag{12b}$$

where body linear velocity error $\delta^B\mathbf{v}$ is rewritten as a function of the INS state errors $\delta^B\mathbf{v} \coloneqq \hat{\mathcal{R}}'\hat{\mathbf{v}} - \mathcal{R}'\mathbf{v} \approx \mathcal{R}'(\mathbf{v})_\times\delta\boldsymbol{\lambda} + \mathcal{R}'\delta\mathbf{v}$.

The angular velocity information expressed in (8a) is exploited by modeling the error dynamics (12a) in the EKF, and feeding the angular velocity measurement to the filter

$$\mathbf{z}_\omega \coloneqq \hat{\boldsymbol{\omega}} = \boldsymbol{\omega} - \delta\mathbf{b}_\omega + \mathbf{n}_\omega. \tag{13}$$

The dynamics of ${}^B\mathbf{v}$ expressed in (8b) are exploited by feeding the filter with the measurement residual

$$\mathbf{z}_v \coloneqq f_v(\hat{\boldsymbol{\omega}}, {}^B\hat{\mathbf{v}}, \hat{\mathcal{R}}, \hat{\mathbf{f}}_{th}) - {}^B\dot{\hat{\mathbf{v}}}, \tag{14}$$

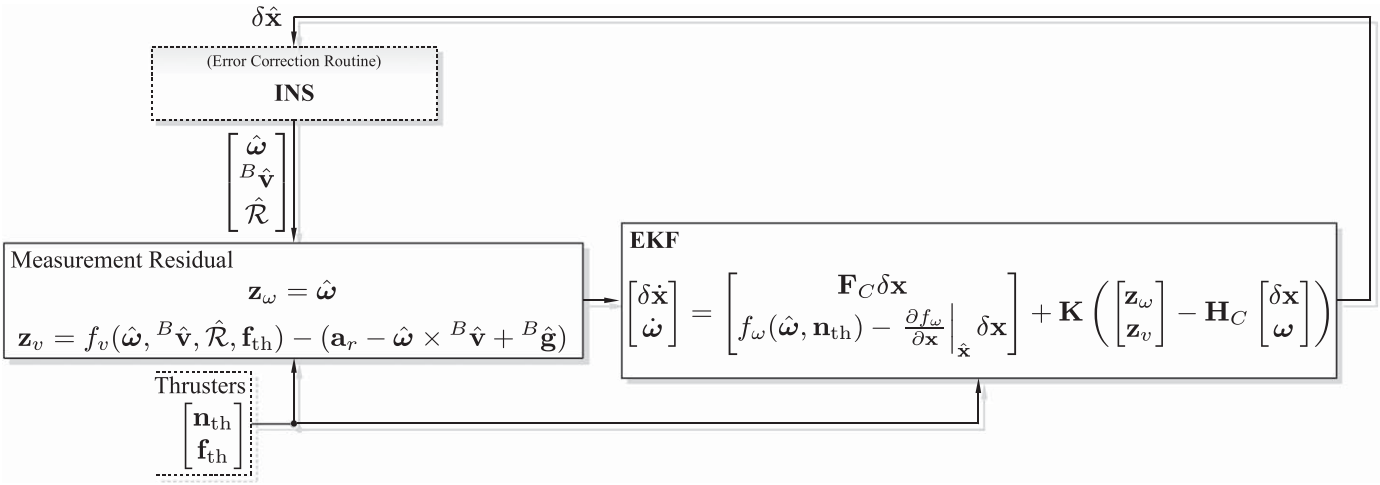

Fig. 3. Embedded vehicle model aiding for the 6-DOF rigid body polyhedron.

where $f_v(\hat{\boldsymbol{\omega}}, {}^{B}\hat{\mathbf{v}}, \hat{\mathcal{R}}, \hat{\mathbf{f}}_{\text{th}})$ is given by computing (8b) with the inertial estimates. The estimate $\hat{\mathbf{v}}$ is obtained from the INS measurements and estimates by rewriting the accelerometer measurement (2b) as the sum of the linear acceleration and Coriolis terms

$$\mathbf{a}_r = \frac{\mathrm{d}^{B}\mathbf{v}}{\mathrm{dt}} + \boldsymbol{\omega} \times {}^{B}\mathbf{v} - \mathcal{R}'^{E}\mathbf{g} - \delta\mathbf{b}_a + \mathbf{n}_a,$$

yielding

$$\frac{\mathrm{d}^{B}\hat{\mathbf{v}}}{\mathrm{dt}} = \mathbf{a}_r - \hat{\boldsymbol{\omega}} \times {}^{B}\hat{\mathbf{v}} + \hat{\mathcal{R}}'^{E}\mathbf{g}.$$

The measurement residual $\mathbf{z}_v$ is formulated in the EKF using a linearized model, that is obtained by expanding (14) as follows:

$$\begin{aligned}\mathbf{z}_v &= f_v(\hat{\boldsymbol{\omega}}, {}^{B}\hat{\mathbf{v}}, \hat{\mathcal{R}}, \hat{\mathbf{f}}_{\text{th}}) - (\mathbf{a}_r - \hat{\boldsymbol{\omega}} \times {}^{B}\hat{\mathbf{v}} + \hat{\mathcal{R}}'^{E}\mathbf{g})\\ &\approx f_v(\hat{\boldsymbol{\omega}}, {}^{B}\hat{\mathbf{v}}, \hat{\mathcal{R}}, \hat{\mathbf{f}}_{\text{th}}) - (f_v(\boldsymbol{\omega}, {}^{B}\mathbf{v}, \mathcal{R}, \mathbf{f}_{\text{th}}) - \delta(\boldsymbol{\omega} \times {}^{B}\mathbf{v}) + \delta^{B}\mathbf{g} - \delta\mathbf{b}_a + \mathbf{n}_a).\end{aligned}$$

Using the first order expansion (12b) and applying the perturbational method described in Britting (1971), produces

$$\begin{aligned}\mathbf{z}_v = &\left((\boldsymbol{\omega})_\times + \frac{\partial f_v}{\partial {}^{B}\mathbf{v}}\right)\mathcal{R}'\delta\mathbf{v} + \left((\boldsymbol{\omega})_\times({}^{B}\mathbf{v})_\times - ({}^{B}\mathbf{g})_\times + \frac{\partial f_v}{\partial {}^{B}\mathbf{v}}({}^{B}\mathbf{v})_\times + \frac{\partial f_v}{\partial \delta\boldsymbol{\lambda}}\mathcal{R}\right)\mathcal{R}'\delta\boldsymbol{\lambda}\\ &+ \delta\mathbf{b}_a + \left(({}^{B}\mathbf{v})_\times - \frac{\partial f_v}{\partial \boldsymbol{\omega}}\right)\delta\mathbf{b}_\omega - \mathbf{n}_a + \left(\frac{\partial f_\omega}{\partial \boldsymbol{\omega}} - ({}^{B}\mathbf{v})_\times\right)\mathbf{n}_\omega.\end{aligned}$$

A block diagram of the embedded vehicle model aiding technique is presented in Fig. 3. The propagation of the vehicle dynamics using INS estimates allows for valuable computational savings and flexibility. Namely, in the embedded VD aiding (i) the number of filter states is smaller than that of the external VD aiding, since the linear velocity information is used in the form of measurement residual (14), and the attitude kinematics are computed using the INS algorithm, (ii) numerical integration methods are necessary only for the computation of (9a), while the linear velocity information is used without integrating the differential equation (9b), and the attitude kinematics (9c) are computed by the INS, (iii) the angular and linear velocity aiding can be implemented separately, i.e. (9a) and (9b) can be exploited independently, whereas the external VD aiding requires the computation of the full vehicle dynamics (9) (iv) error compensation routines are only performed in the INS, as opposed to implementing error compensation routines associated with the external vehicle model aiding. From the viewpoint of algebraic derivation, the Jacobians computed for the embedded VD aiding are also computed in the classical method, see (10), and hence the first order analytical results needed to integrate the vehicle model in the EKF are the same for both architectures. The computational advantages of the embedded vehicle model are illustrated in the simulation results presented later in this work.

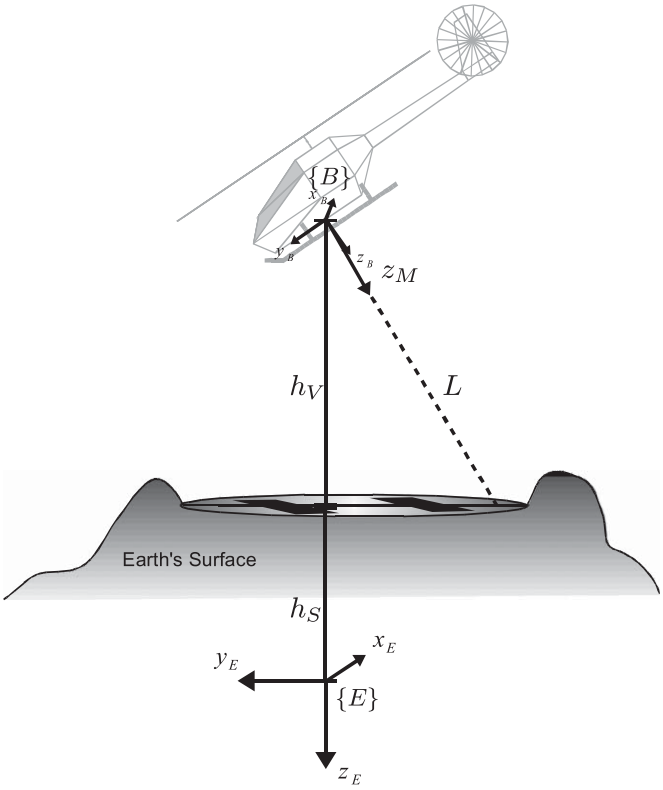

Fig. 4. LASER range finder reading (${}^{B}_{M}\mathbf{R} = \mathbf{I}$).

4. LASER aiding

In this section, the LASER range finder aiding sensor is described and the corresponding filter observation equation is introduced. By definition, and without loss of generality, the sensor is mounted along the z-axis of the frame $\{M\}$, whose relative orientation to the body frame is described by the known

installation rotation matrix ${}^{B}_{M}\mathbf{R}$, for calibration methods see Guerreiro, Silvestre, Oliveira, and Vasconcelos (2008) and references therein. The LASER reads the distance L from the vehicle to the ground, along the z-axis of the $\{M\}$ coordinate frame, as depicted in Fig. 4. By processing this information in the filter architecture, an estimate of the vehicle's distance to the ground can be obtained with high accuracy, as required for landing and takeoff operations of an air vehicle.

In the current work, the landing area is assumed to be locally planar. The ground height h_S, given by the distance from the Earth frame origin to the helicopter landing zone, is modeled as being approximately constant

$$\dot{h}_S = n_{h_S}, \tag{15}$$

where $n_{h_S} \sim \mathcal{N}(0, \Xi_{h_S})$ is a Gaussian white noise process whose variance reflects small variations on the ground's flatness. As depicted in Fig. 4, the z-axis Earth coordinate of the vehicle is given by

$$p_z = -(h_S + h_V), \tag{16}$$

where $h_V \geq 0$ is the vehicle's height, that is, the distance from Body frame origin to the ground.

Using elementary trigonometric relations yields $h_V/L = |{}^{M}\mathbf{h}_V'\mathbf{e}_z|/|{}^{E}\mathbf{h}_V'\mathbf{e}_z|$, where ${}^{E}\mathbf{h}_V = [0\ 0\ -h_V]'$ is the vehicle's height in Earth coordinates, $\mathbf{e}_z = [0\ 0\ 1]'$ is the unitary z-axis vector and ${}^{E}\mathbf{h}_V'\mathbf{e}_z$ corresponds to the projection of $\mathbf{h}_V$ on the z-axis of the $\{M\}$ frame. Applying the coordinate transform ${}^{M}\mathbf{h}_V = {}^{B}_{M}\mathbf{R}'\mathcal{R}'{}^{E}\mathbf{h}_V$ and developing the terms in the previous equation, the LASER range is described by

$$L = \frac{h_V}{\mathbf{e}_z'\mathcal{R}_M^B\mathbf{R}\mathbf{e}_z} \quad \text{if } \mathbf{e}_z'\mathcal{R}_M^B\mathbf{R}\mathbf{e}_z > 0, \tag{17}$$

that is not defined for the cases where the LASER is pointing upwards $\mathbf{e}_z'\mathcal{R}_M^B\mathbf{R}\mathbf{e}_z \leq 0$. The LASER range finder sensor measures the actual range L corrupted by the sensor noise

$$L_r = L + \delta L, \tag{18}$$

where $\delta L = n_L \sim \mathcal{N}(0, \Xi_L)$ is modeled as a Gaussian white noise process. The measurement residual is computed by

$$\mathbf{z}_L \coloneqq \hat{p}_z - (-\hat{h}_V), \tag{19}$$

where the height estimate from the LASER reading is given by rearranging the terms in (17) and using the INS estimates in the unknown terms, producing

$$\hat{h}_V = \mathbf{e}_z'\hat{\mathcal{R}}_M^B\mathbf{R}\mathbf{e}_z L_r. \tag{20}$$

The vehicle and ground heights, h_S and h_V, respectively, are filtered apart by modeling the h_S dynamics (15) in the EKF, measuring h_V from the LASER reading as in (20), and feeding the measurement residual (19) to the EKF.

To model the measurement residual (19) in the EKF, the INS position estimate is expressed as a function of the vehicle and ground heights, given by

$$\hat{p}_z = p_z + \delta p_z = -h_S - h_V + \mathbf{e}_z'\delta\mathbf{p}.$$

Expanding the INS attitude estimate $\hat{\mathcal{R}}$ with the attitude error approximation (4) and neglecting second order terms yields the $\hat{h}_V$ description

$$\begin{aligned}\hat{h}_V &= \mathbf{e}_z'\hat{\mathcal{R}}_M^B\mathbf{R}\mathbf{e}_z L_r \approx \mathbf{e}_z'[\mathbf{I}_3 + (\delta\boldsymbol{\lambda})_\times]\mathcal{R}_M^B\mathbf{R}\mathbf{e}_z L_r \\ &\approx \mathbf{e}_z'\mathcal{R}_M^B\mathbf{R}\mathbf{e}_z(L+\delta L) - L_r\mathbf{e}_z'(\mathcal{R}_M^B\mathbf{R}\mathbf{e}_z)_\times\delta\boldsymbol{\lambda} \\ &= h_V + \mathbf{e}_z'\mathcal{R}_M^B\mathbf{R}\mathbf{e}_z\delta L - L_r\mathbf{e}_z'(\mathcal{R}_M^B\mathbf{R}\mathbf{e}_z)_\times\delta\boldsymbol{\lambda}.\end{aligned} \tag{21}$$

Combining (18)–(21), the measurement residual is described as a function of the EKF state variables as

$$\mathbf{z}_L = \mathbf{e}_z'\delta\mathbf{p} - L_r\mathbf{e}_z'(\mathcal{R}_M^B\mathbf{R}\mathbf{e}_z)_\times\delta\boldsymbol{\lambda} - h_S + \mathbf{e}_z'\mathcal{R}_M^B\mathbf{R}\mathbf{e}_z\mathbf{n}_L. \tag{22}$$

In practical applications, the terrain height h_S is unknown along the flight path. After the takeoff and during flight operations, the LASER sensor is switched off to prevent erroneous readings due to the terrain height fluctuations, and to the interference of obstacles located between the vehicle and the ground. When the landing maneuver starts, the LASER is switched on to estimate the new h_S and the distance-to-ground.

5. Implementation

This section details the state model of the EKF, that integrates the INS with the vehicle model and LASER aiding techniques. The state dynamics and measurement residuals of the EKF are determined by the choice of aiding techniques, and obtained by the concatenation of the INS error model presented in Section 2 with the state and measurement models of the aiding sources described in Sections 3 and 4. The state models for the external and the embedded vehicle model aiding techniques evidence the differences between the two approaches, and clarify the computational savings and flexibility of the proposed technique. The discretization of the continuous state space model and the Kalman filter algorithm are presented for the purpose of implementation.

The standard continuous-time state space model can be described by

$$\dot{\mathbf{x}}_C = \mathbf{F}_C(\mathbf{x}_C)\mathbf{x}_C + \mathbf{G}_C(\mathbf{x}_C)\mathbf{n}_{x_C} + \mathbf{u}_C, \quad \mathbf{z}_C = \mathbf{H}_C(\mathbf{x}_C)\mathbf{x}_C + \mathbf{n}_{z_C}, \tag{23}$$

where $\mathbf{x}_C$ is the state vector, $\mathbf{F}_C$ is the state dynamics matrix, $\mathbf{n}_{x_C}$ is the state noise transformed by matrix $\mathbf{G}_C$, $\mathbf{u}_C$ is the system input vector, and $\mathbf{z}$ is the state measurement, corrupted by the noise vector $\mathbf{n}_{z_C}$. The state and measurement noises are modeled as zero-mean, Gaussian white noise processes with covariance matrices denoted by $\mathbf{Q}_C$ and $\mathbf{R}_C$, respectively.

5.1. INS/EKF state model

The state model dynamics for the INS errors are obtained directly from (5). Let $\mathbf{x}_{\text{INS}} = (\mathbf{p}, \mathbf{v}, \mathcal{R}, \mathbf{b}_a, \mathbf{b}_\omega)$ denote the INS quantities, the state model dynamics of the EKF describing the INS errors are given by

$$\dot{\delta}\mathbf{x} = \mathbf{F}_I(\mathbf{x}_{\text{INS}})\delta\mathbf{x} + \mathbf{G}_I(\mathbf{x}_{\text{INS}})\mathbf{n}_{\text{INS}}, \tag{24}$$

where

$$\delta\mathbf{x} = [\delta\mathbf{p}'\ \ \delta\mathbf{v}'\ \ \delta\boldsymbol{\lambda}'\ \ \delta\mathbf{b}_a'\ \ \delta\mathbf{b}_\omega']', \quad \mathbf{n}_{\text{INS}} = [\mathbf{n}_p'\ \ \mathbf{n}_a'\ \ \mathbf{n}_\omega'\ \ \mathbf{n}_{b_a}'\ \ \mathbf{n}_{b_\omega}']',$$

$$\mathbf{F}_I(\mathbf{x}_{\text{INS}}) = \begin{bmatrix} \mathbf{0} & \mathbf{I}_3 & \mathbf{0} & \mathbf{0} & \mathbf{0} \\ \mathbf{0} & \mathbf{0} & -(\mathcal{R}\mathbf{a}_r)_\times & -\mathcal{R} & \mathbf{0} \\ \mathbf{0} & \mathbf{0} & \mathbf{0} & \mathbf{0} & -\mathcal{R} \\ \mathbf{0} & \mathbf{0} & \mathbf{0} & \mathbf{0} & \mathbf{0} \\ \mathbf{0} & \mathbf{0} & \mathbf{0} & \mathbf{0} & \mathbf{0} \end{bmatrix},$$

$$\mathbf{G}_I(\mathbf{x}_{\text{INS}}) = \text{blkdiag}(\mathbf{I}_3, \mathcal{R}, \mathcal{R}, -\mathbf{I}_3, -\mathbf{I}_3),$$

where blkdiag(...) represents a block diagonal matrix, $\mathbf{n}_p \sim \mathcal{N}(\mathbf{0}, \boldsymbol{\Xi}_p)$ is a Gaussian white noise process associated with the position error estimate and the state noise covariance matrix is given by

$$\mathbf{Q}_{\text{INS}} = \text{blkdiag}(\boldsymbol{\Xi}_p, \boldsymbol{\Xi}_a, \boldsymbol{\Xi}_\omega, \boldsymbol{\Xi}_{b_a}, \boldsymbol{\Xi}_{b_\omega}).$$

The measurement model for the proposed VD and LASER aiding techniques is described in the ensuing, however additional information sources are considered. A GPS receiver

and a magnetometer are integrated in the system using the measurement residuals

$$\mathbf{z}_{\text{GPS}} \coloneqq \hat{\mathbf{p}} - \mathbf{p}_{\text{GPS}} \approx \delta\mathbf{p} - \mathbf{n}_{\text{GPS}},$$
$$\mathbf{z}_m \coloneqq {}^{E}\mathbf{m} - \hat{\mathcal{R}}\mathbf{m}_r \approx ({}^{E}\mathbf{m})_{\times}\delta\boldsymbol{\lambda} - \mathcal{R}\mathbf{n}_m, \tag{25}$$

where $\mathbf{p}_{\text{GPS}}$ is the position measured by the GPS unit, $\mathbf{m}_r$ is the magnetometer reading, ${}^{E}\mathbf{m}$ represents the Earth's magnetic field in Earth coordinates, and $\mathbf{n}_{\text{GPS}} \sim \mathcal{N}(\mathbf{0}, \Xi_{\text{GPS}})$, $\mathbf{n}_m \sim \mathcal{N}(\mathbf{0}, \Xi_m)$ are Gaussian white noise processes. For further details on the derivation of the measurement residuals (25), the reader is referred to (Britting, 1971; Markley, 2003; Vasconcelos et al., 2005).

5.2. Vehicle model aiding

The EKF state space model, formulated using (23), is obtained by concatenating the state space model (24) that describes the INS estimation errors, with the state model and measurements of the vehicle model aiding techniques described in Sections 3.2 and 3.3. With a slight abuse of notation, the state model (23) is defined for the external and embedded vehicle model dynamics using the same state $\mathbf{x}_C$ and measurement $\mathbf{z}_C$ variables.

5.2.1. External vehicle model aiding

In the external vehicle model aiding technique, the vehicle dynamics are computed by a self-contained VD simulator as shown in Fig. 2, and consequently the INS and the VD states are distinct. As a mean to estimate and compensate for the INS errors, the EKF state model is augmented with the VD error dynamics (9), and the measurement residuals (11) are a linear combination of the INS and the VD errors. The classical VD aiding methodology requires specific computational routines to compensate for the estimation errors in the VD simulator.

The continuous-time error state space model for the navigation system with external VD aiding is obtained directly from the EKF/INS state model (24) augmented with the VD error dynamics (9), yielding

$$\mathbf{x}_C \coloneqq [\delta\mathbf{x}' \;\; \delta\mathbf{x}_{\text{V}}']', \quad \mathbf{n}_{x_C} \coloneqq [\mathbf{n}_{\text{INS}}' \;\; \mathbf{n}_{x_{\text{V}}}']', \quad \mathbf{u}_C = \mathbf{0},$$

$$\mathbf{F}_C(\mathbf{x}_{\text{INS}}, \mathbf{x}_{\text{V}}) = \begin{bmatrix} \mathbf{F}_I(\mathbf{x}_{\text{INS}}) & \mathbf{0}_{15\times 9} \\ \mathbf{0}_{9\times 15} & \mathbf{F}_{\text{V}}(\mathbf{x}_{\text{V}}) \end{bmatrix}, \quad \mathbf{G}_C(\mathbf{x}_{\text{INS}}) = \begin{bmatrix} \mathbf{G}_I(\mathbf{x}_{\text{INS}}) & \mathbf{0}_{15\times 9} \\ \mathbf{0}_{9\times 15} & \mathbf{G}_{\text{V}} \end{bmatrix},$$

with the vehicle states, noises and model submatrices given by

$$\delta\mathbf{x}_{\text{V}} \coloneqq [\delta\boldsymbol{\omega}_{\text{V}}' \;\; \delta{}^{B}\mathbf{v}_{\text{V}}' \;\; \delta\boldsymbol{\lambda}_{\text{V}}']', \quad \mathbf{n}_{x_{\text{V}}} \coloneqq [\mathbf{n}_{\boldsymbol{\omega}_{\text{V}}}' \;\; \mathbf{n}_{\mathbf{v}_{\text{V}}}' \;\; \mathbf{n}_{\boldsymbol{\lambda}_{\text{V}}}']',$$

$$\mathbf{F}_{\text{V}}(\mathbf{x}_{\text{V}}) = \left.\begin{bmatrix} \frac{\partial f_\omega}{\partial \boldsymbol{\omega}} & \mathbf{0} & \mathbf{0} \\ \frac{\partial f_v}{\partial \boldsymbol{\omega}} & \frac{\partial f_v}{\partial {}^{B}\mathbf{v}} & \frac{\partial f_v}{\partial \boldsymbol{\lambda}} \\ \mathcal{R}_{\text{V}} & \mathbf{0} & \mathbf{0} \end{bmatrix}\right|_{\mathbf{x}_{\text{V}}}, \quad \mathbf{G}_{\text{V}} = \begin{bmatrix} \mathbf{I} & \mathbf{0} & \mathbf{0} \\ \mathbf{0} & \mathbf{I} & \mathbf{0} \\ \mathbf{0} & \mathbf{0} & \mathbf{I} \end{bmatrix},$$

where $\mathbf{n}_{\boldsymbol{\omega}_{\text{V}}}$, $\mathbf{n}_{\mathbf{v}_{\text{V}}}$, and $\mathbf{n}_{\boldsymbol{\lambda}_{\text{V}}}$ are zero-mean, Gaussian white noise processes with covariances $\Xi_{\boldsymbol{\omega}_{\text{V}}}$, $\Xi_{\mathbf{v}_{\text{V}}}$, and $\Xi_{\boldsymbol{\lambda}_{\text{V}}}$ respectively, that characterize the vehicle modeling errors.

The measurement residuals (11) are a function of the INS and VD errors, given in the state space form by

$$\mathbf{z}_C \coloneqq [\mathbf{z}_\omega' \;\; \mathbf{z}_u' \;\; \mathbf{z}_{\mathcal{R}}']', \quad \mathbf{n}_{z_{\text{V}}} \coloneqq [\mathbf{n}_\omega' + \mathbf{n}_{\mathbf{z}_\omega}' \;\; \mathbf{n}_{\mathbf{z}_u}' \;\; \mathbf{n}_{\mathbf{z}_{\mathcal{R}}}']',$$

$$\mathbf{H}_C(\mathbf{x}_{\text{INS}}) = \begin{bmatrix} \mathbf{0} & \mathbf{0} & \mathbf{0} & \mathbf{0} & -\mathbf{I} & -\mathbf{I} & \mathbf{0} & \mathbf{0} \\ \mathbf{0} & \mathcal{R}' & \mathcal{R}'(\mathbf{v})_{\times} & \mathbf{0} & \mathbf{0} & \mathbf{0} & -\mathbf{I} & \mathbf{0} \\ \mathbf{0} & \mathbf{0} & \mathbf{I} & \mathbf{0} & \mathbf{0} & \mathbf{0} & \mathbf{0} & -\mathbf{I} \end{bmatrix},$$

where $\mathbf{n}_{z_\omega}$, $\mathbf{n}_{z_U}$, and $\mathbf{n}_{z_{\mathcal{R}}}$ are zero-mean Gaussian white noise processes associated with the $\delta\mathbf{z}_{\text{V}}$ observation, with covariances Ξ_{z_ω}, Ξ_{z_U}, and $\Xi_{z_{\mathcal{R}}}$ respectively. The vehicle states and measurements noise covariance matrices are

$$\mathbf{Q}_C = \text{blkdiag}(\mathbf{Q}_{\text{INS}}, \Xi_{\omega_{\text{V}}}, \Xi_{u_{\text{V}}}, \Xi_{\mathcal{R}_{\text{V}}}), \quad \mathbf{R}_C = \text{blkdiag}(\Xi_{z_\omega} + \Xi_\omega, \Xi_{z_u}, \Xi_{z_{\mathcal{R}}}),$$

where the white noise variances account for the effects of neglecting high order terms and unmodeled uncertainties in the measurement residual derivation.

The observation $\mathbf{z}_\omega$ is disturbed by rate gyro noise, so a state and measurement noise correlation matrix is introduced in the Kalman filter equations

$$\mathbf{C}_C = \begin{bmatrix} \mathbf{0} & \mathbf{0} & \Xi_\omega & \mathbf{0} & \mathbf{0} & \mathbf{0}_{3\times 9} \\ & & \mathbf{0}_{6\times 15} & & & \mathbf{0}_{6\times 9} \end{bmatrix}',$$

for details on the definition and derivation see (Brown & Hwang, 1997) and references therein.

As presented in Table 1, the external vehicle model aiding increases the EKF dimensionality by 9 states, and propagate $f_\omega(\boldsymbol{\omega}, \mathbf{n}_{\text{th}})$, $f_v(\boldsymbol{\omega}_V, {}^{B}\mathbf{v}_V, \mathbf{f}_{\text{th}})$, and $f_{\mathcal{R}}(\boldsymbol{\omega}_V, \mathcal{R}_V)$ although the latter is also computed by the inertial integration algorithm. As discussed in Section 3.3, the proposed embedded VD aiding technique reduces the computational cost of vehicle model integration, by requiring a smaller state space augmentation and by propagating only the necessary vehicle model differential equations.

Table 1
Comparison of the vehicle model aiding techniques with a standard GPS aided IMU.

	Aiding technique		
	GPS	External VD	Embedded VD
EKF state space dimension	15	24	18
Propagated VD equations	–	$f_\omega(\boldsymbol{\omega}, \mathbf{n}_{\text{th}})$ $f_v(\boldsymbol{\omega}_V, {}^{B}\mathbf{v}_V, \mathbf{f}_{\text{th}})$ $f_{\mathcal{R}}(\boldsymbol{\omega}_V, \mathcal{R}_V)$	$f_\omega(\boldsymbol{\omega}, \mathbf{n}_{\text{th}})$

5.2.2. Embedded vehicle model aiding

The implementation of the embedded vehicle model aiding technique for the 6 DOF rigid body is illustrated in Fig. 3. In this technique, the VD angular velocity is integrated in the navigation system by augmenting the EKF state model with (12a), propagating $f_\omega(\boldsymbol{\omega}, \mathbf{n}_{\text{th}})$ using the INS estimates, and using the measurement residual (13). The VD linear velocity information is integrated in the filter using the measurement residual (14), where $\mathbf{f}_v(\boldsymbol{\omega}, {}^{B}\mathbf{v}, \mathcal{R}, \mathbf{f}_{\text{th}})$ is computed using the INS estimates. The continuous-time state space model is given by

$$\mathbf{x}_C \coloneqq [\delta\mathbf{x}' \;\; \mathbf{x}_{\text{V}}']', \quad \mathbf{n}_{x_C} \coloneqq [\mathbf{n}_{\text{INS}}' \;\; \mathbf{n}_{x_{\text{V}}}']', \quad \mathbf{u}_C = f_\omega(\boldsymbol{\omega}, \mathbf{n}_{th}),$$

$$\mathbf{F}_C(\mathbf{x}_{\text{INS}}) = \begin{bmatrix} \mathbf{F}_I(\mathbf{x}_{\text{INS}}) & \mathbf{0}_{15\times 3} \\ \mathbf{F}_{\text{V}}(\mathbf{x}_{\text{INS}}) & \mathbf{0}_{3\times 3} \end{bmatrix}, \quad \mathbf{G}_C(\mathbf{x}_{\text{INS}}) = \begin{bmatrix} \mathbf{G}_I(\mathbf{x}_{\text{INS}}) & \mathbf{0}_{9\times 3} \\ \mathbf{G}_{\text{V}}(\mathbf{x}_{\text{INS}}) & \mathbf{I}_3 \end{bmatrix},$$

where

$$\mathbf{x}_{\text{V}} = \boldsymbol{\omega}, \quad \mathbf{n}_{x_{\text{V}}} = \mathbf{n}_{\boldsymbol{\omega}_{\text{V}}}, \quad \mathbf{F}_{\text{V}}(\mathbf{x}_{\text{INS}}) = \left[\mathbf{0} \;\; \mathbf{0} \;\; \mathbf{0} \;\; \mathbf{0} \;\; \left.\frac{\partial f_\omega}{\partial \boldsymbol{\omega}}\right|_{\hat{\mathbf{x}}}\right],$$

$$\mathbf{G}_{\text{V}}(\mathbf{x}_{\text{INS}}) = \left[\mathbf{0} \;\; \mathbf{0} \;\; -\left.\frac{\partial f_\omega}{\partial \boldsymbol{\omega}}\right|_{\hat{\mathbf{x}}} \;\; \mathbf{0} \;\; \mathbf{0}\right],$$

where $\mathbf{n}_{\boldsymbol{\omega}_{\text{V}}}$ is a zero-mean, Gaussian white noise with covariance $\Xi_{\boldsymbol{\omega}_{\text{V}}}$, that characterizes the vehicle modeling errors. The $\mathbf{x}_{\text{V}}$ state variable is propagated using the INS estimates as expressed in (12a), and the EKF state matrices depend only on the INS quantities $\mathbf{x}_{\text{INS}}$, as expected from the derivation of the technique presented in Section 3.3.

The measurement state model (13), (14) is described in the state space form by

$$\mathbf{z} \coloneqq [\mathbf{z}'_\omega \;\; \mathbf{z}'_v]', \quad \mathbf{n}_{z_v} \coloneqq \left[\mathbf{n}'_\omega + \mathbf{n}'_{\mathbf{z}_\omega} \;\; -\mathbf{n}'_a + \left(\left(\frac{\partial f_\omega}{\partial \boldsymbol{\omega}} - ({}^B\mathbf{v})_\times\right)\mathbf{n}_\omega\right)' + \mathbf{n}'_{\mathbf{z}_v}\right]',$$

$$\mathbf{H}_C(\mathbf{x}_{\mathrm{INS}}) = \left[\begin{array}{cccccc} \mathbf{0} & \mathbf{0} & \mathbf{0} & \mathbf{0} & -\mathbf{I} & \mathbf{I} \\ \mathbf{0} & \left((\boldsymbol{\omega})_\times + \dfrac{\partial f_v}{\partial {}^B\mathbf{v}}\right)\mathcal{R}' & \mathbf{H}_{v\mathcal{R}}(\mathbf{x}_{\mathrm{INS}}) & \mathbf{I} & ({}^B\mathbf{v})_\times - \dfrac{\partial f_v}{\partial \boldsymbol{\omega}} & \mathbf{0} \end{array}\right]\Bigg|_{\hat{\mathbf{x}}},$$

where

$$\mathbf{H}_{v\mathcal{R}}(\mathbf{x}_{\mathrm{INS}}) \coloneqq \left((\boldsymbol{\omega})_\times ({}^B\mathbf{v})_\times - ({}^B\mathbf{g})_\times + \frac{\partial f_v}{\partial {}^B\mathbf{v}}({}^B\mathbf{v})_\times + \frac{\partial f_v}{\partial \delta\boldsymbol{\lambda}}\mathcal{R}\right)\mathcal{R}',$$

and $\mathbf{n}_{\mathbf{z}_\omega} \sim \mathcal{N}(\mathbf{0}, \Xi_{z_\omega})$ and $\mathbf{n}_{\mathbf{z}_v} \sim \mathcal{N}(\mathbf{0}, \Xi_{z_u})$ are zero-mean Gaussian white noise processes associated with the measurement. The vehicle states and measurements noise covariance and covariance correlation matrices are given by

$$\mathbf{Q}_C = \mathrm{blkdiag}(\mathbf{Q}_{\mathrm{INS}}, \Xi_{\omega_v}),$$

$$\mathbf{R}_C = \mathrm{blkdiag}\left(\Xi_\omega + \Xi_{z_\omega}, \Xi_a + \left(\frac{\partial f_\omega}{\partial \boldsymbol{\omega}} - ({}^B\mathbf{v})_\times\right)\Xi_\omega\left(\frac{\partial f_\omega}{\partial \boldsymbol{\omega}} - ({}^B\mathbf{v})_\times\right)' + \Xi_{z_v}\right),$$

$$\mathbf{C}_C = \left[\begin{array}{cccccc} \mathbf{0} & \mathbf{0} & \Xi_\omega & \mathbf{0} & \mathbf{0} & \mathbf{0}_{3\times 3} \\ \mathbf{0} & -\Xi_a & \left(\dfrac{\partial f_\omega}{\partial \boldsymbol{\omega}} - ({}^B\mathbf{v})_\times\right)\Xi_\omega & \mathbf{0} & \mathbf{0} & \mathbf{0}_{3\times 3} \end{array}\right]'.$$

The number of EKF states for the embedded VD aiding is smaller than that of the external VD aiding, as evidenced in Table 1, due to the use of $f_v(\hat{\boldsymbol{\omega}}, {}^B\hat{\mathbf{v}}, \hat{\mathcal{R}}, \hat{\mathbf{f}}_{\mathrm{th}})$ directly in the measurement (14) and to the propagation of the attitude kinematics using the INS. The computational cost of using VD model is also smaller because numerical integration methods are only adopted to solve for $f_\omega(\hat{\omega}, \hat{\mathbf{n}}_{\mathrm{th}})$. Moreover, the angular velocity and linear velocity aiding can be independently enabled or disabled, contrary to the external VD aiding, by including or omitting $\mathbf{z}_\omega$ and $\mathbf{z}_v$ respectively.

5.3. LASER aiding

The LASER sensor is integrated with the INS by defining the variables and matrices of the EKF state model (23) as

$$\mathbf{x}_C \coloneqq [\delta\mathbf{x}' \;\; h_S]', \quad \mathbf{n}_{x_C} \coloneqq [\mathbf{n}'_{\mathrm{INS}} \;\; n_{h_S}]', \quad \mathbf{u}_C = \mathbf{0},$$

$$\mathbf{F}_C(\mathbf{x}_{\mathrm{INS}}) = \begin{bmatrix} \mathbf{F}_I(\mathbf{x}_{\mathrm{INS}}) & \mathbf{0}_{15\times 1} \\ \mathbf{0}_{1\times 15} & 0 \end{bmatrix}, \quad \mathbf{G}_C(\mathbf{x}_{\mathrm{INS}}) = \begin{bmatrix} \mathbf{G}_I(\mathbf{x}_{\mathrm{INS}}) & \mathbf{0}_{9\times 1} \\ \mathbf{0}_{1\times 9} & 1 \end{bmatrix}.$$

The measurement model is obtained from (22) and given by

$$\mathbf{z}_C \coloneqq \mathbf{z}_L, \quad \mathbf{n}_{z_C} \coloneqq \mathbf{n}_{z_L},$$

$$\mathbf{H}_C(\mathbf{x}_{\mathrm{INS}}) = [\mathbf{e}'_z \;\; \mathbf{0}_{1\times 3} \;\; -\mathbf{e}'_z(\mathcal{R}^B_M \mathbf{R}\mathbf{e}_z)_\times \;\; \mathbf{0}_{1\times 3} \;\; \mathbf{0}_{1\times 3} \;\; -1],$$

where

$$\mathbf{Q}_C = \mathrm{blkdiag}(\mathbf{Q}_{\mathrm{INS}}, \Xi_{h_S}), \quad \mathbf{R}_C = (\mathbf{e}'_z \mathcal{R}^B_M \mathbf{R}\mathbf{e}_z)^2 \Xi_L, \quad \mathbf{C}_C = \mathbf{0}.$$

The LASER sensor is adopted for takeoff and landing maneuvers. Previous to the LASER's activation, the estimation covariance of h_S is defined large enough to account for the uncertainty in the terrain height. When the LASER sensor is activated, the EKF recursively estimates the terrain height h_S based on the sensor measurements, and the uncertainty on the terrain's height converges asymptotically to a steady state value, that depends on the sensor's accuracy.

When the LASER is switched off, the uncertainty on the terrain height h_S will grow at a rate defined by the noise covariance Ξ_{h_S}. Techniques to avoid numerical problems in the EKF covariance matrices should be adopted, namely square root filtering (Brown & Hwang, 1997) or by setting $\Xi_{h_S} = 0$ if the uncertainty reaches a specific upper bound.

5.4. Discrete-time implementation

The discrete-time equivalent of the state space model (23) can be obtained using the classical zero-order hold discretization method detailed in (Brown & Hwang, 1997) and in references therein. In this approach, the discrete-time state and measurement covariance matrices are approximated by $\mathbf{Q}_k \simeq [\mathbf{G}_k \mathbf{Q}_{Ck} \mathbf{G}'_k]T$, $\mathbf{R}_k \simeq \mathbf{R}_{Ck}/T$ where T is the sampling period, $\mathbf{G}_k = \mathbf{G}_C|_{t=t_k}$, $\mathbf{Q}_{Ck} = \mathbf{Q}_C\big|_{t=t_k}$, and $\mathbf{R}_{Ck} = \mathbf{R}_C|_{t=t_k}$. The discrete-time equivalent for the correlation matrix $\mathbf{C}_C$ is harder to find in the literature, but can be derived using the same principles adopted for $\mathbf{Q}_k$ and $\mathbf{R}_k$, yielding

$$\mathbf{C}_k = \frac{1}{T}\int_{t_{k-1}}^{t_k} \boldsymbol{\Phi}(t_{k+1}, \theta)\mathbf{G}_C(\tau)\mathbf{C}_C(\tau)\,d\tau \approx \left(\mathbf{I} + \frac{\mathbf{F}_k T}{2} + \frac{\mathbf{F}_k^2 T^2}{6}\right)\mathbf{G}_k \mathbf{C}_{Ck},$$

where $\mathbf{F}_k = \mathbf{F}_C|_{t=t_k}$ and $\mathbf{C}_{Ck} = \mathbf{C}_C|_{t=t_k}$. The recursive EKF equations for discrete-time systems are thoroughly documented in the literature (Gelb, 1974; Brown & Hwang, 1997). In the adopted direct feedback configuration, shown in Fig. 1, the position and attitude estimates stored in the INS are updated using the EKF error estimates as follows

$$\hat{\mathbf{p}}_k^+ = \hat{\mathbf{p}}_k^- - \delta\hat{\mathbf{p}}_k, \quad \hat{\mathbf{v}}_k^+ = \hat{\mathbf{v}}_k^- - \delta\hat{\mathbf{v}}_k, \quad \hat{\mathcal{R}}_k^+ = \mathcal{R}'(\delta\hat{\boldsymbol{\lambda}}_k)\hat{\mathcal{R}}_k^-, \tag{26a}$$

$$\hat{\mathbf{b}}_{ak}^+ = \hat{\mathbf{b}}_{ak}^- - \delta\hat{\mathbf{b}}_{ak}, \quad \hat{\mathbf{b}}_{\omega k}^+ = \hat{\mathbf{b}}_{\omega k}^- - \delta\hat{\mathbf{b}}_{\omega k}, \tag{26b}$$

where the $-$ and $+$ superscripts denote respectively the quantities before and after the update using the measurement $\mathbf{z}_k$, and matrix $\mathcal{R}'(\delta\hat{\boldsymbol{\lambda}}_k)$ is implemented using power series expansion of trigonometric terms up to an arbitrary accuracy (Savage, 1998a). This procedure updates the linearization point and keeps filter perturbational dynamics valid under the first order assumptions. The EKF error estimates are reset after being applied to compensate the INS states, i.e. the error estimates are set as $\delta\hat{\mathbf{p}}_k = \delta\hat{\mathbf{v}}_k = \delta\hat{\boldsymbol{\lambda}}_k = \delta\hat{\mathbf{b}}_{a\,k} = \delta\hat{\mathbf{b}}_{\omega k} = \mathbf{0}$ after computing (26).

Note that the derivation of the external vehicle model aiding technique is similar to that adopted for the INS, and hence it is necessary to feed back the estimated VD errors as shown in Figs. 1(a) and 2. The VD error compensation routines are described by

$$\hat{\boldsymbol{\omega}}_{\mathrm{V}k}^+ = \hat{\boldsymbol{\omega}}_{\mathrm{V}k}^- - \delta\hat{\boldsymbol{\omega}}_{\mathrm{V}k}, \quad {}^B\hat{\mathbf{v}}_{\mathrm{V}k}^+ = {}^B\hat{\mathbf{v}}_{\mathrm{V}k}^- - \delta^B\hat{\mathbf{v}}_{\mathrm{V}k}, \quad \hat{\mathcal{R}}_{\mathrm{V}k}^+ = \hat{\mathcal{R}}'_{\mathrm{V}k}(\delta\hat{\boldsymbol{\lambda}}_{\mathrm{V}})\hat{\mathcal{R}}_{\mathrm{V}k}^-.$$

By construction, the embedded VD technique propagates some vehicle dynamics using the EKF state space. Vehicle model error compensation routines are not necessary in this technique, since the estimation error compensation is automatically performed by the EKF in the state update step.

6. Simulation results

This section presents the simulations results that validate and illustrate the properties of the proposed aiding techniques. The

Table 2
Sensor non-idealities.

Sensor	Bias	Noise variance
Rate Gyro	$0.05^\circ/\mathrm{s}$	$(0.02^\circ/\mathrm{s})^2$
Accelerometer	10 mg	$(0.6\,\mathrm{mg})^2$
LASER	–	$(10^{-2}\,\mathrm{m})^2$
Magnetometer	–	$(1\,\mathrm{mG})^2$
GPS	–	$10\,\mathrm{m}^2$

integration of the VD and LASER range finder information in the navigation system is studied using three simulation setups. The first simulation compares the estimation results of the VD aided navigation system with those obtained using a classical GPS/INS architecture, for a 6-DOF rigid body describing a trimming trajectory, and the embedded VD aiding technique is validated with respect to the classical VD aided navigation system.

In the second simulation, the proposed VD aiding is applied for the case of a model-scale Vario X-Treme helicopter, to demonstrate the implementation of the technique for highly nonlinear, realistic vehicle models. Simulation results are presented for a takeoff and turning trajectory, and the estimation results of a GPS based and the VD aided navigation architectures are analyzed.

The third simulation emphasizes the role of the LASER range finder sensor for critical maneuvers. The vehicle describes a hovering maneuver, and has to acquire the distance-to-ground for automatic landing. Accuracy improvements obtained with the LASER range finder sensor integrated on a GPS/INS configuration are evidenced. Dynamic estimation of distance-to-ground is performed, and position and velocity vertical channel accuracy enhancements are shown.

The INS high speed algorithm is set to run at 100 Hz and the normal speed algorithm is synchronized with the EKF, both executed at 50 Hz. The LASER sensor operates at 10 Hz and the GPS provides position measurements at the nominal frequency of 1 Hz. Table 2 characterizes the non-idealities of the low-cost sensor unit integrated in the robotic platforms.

Table 3
Rigid body characteristics.

Property	Nominal value
Mass	$m = 10\,\text{kg}$
Length, width, height	$(l, w, h) = (1.00, 0.75, 0.25)\,\text{m}$
Rear thrusters position	${}^{B}\mathbf{p}_{\text{th1,2}} = [-0.50 \;\; \pm 0.30 \;\; 0]\,\text{m}$
Side thrusters position	${}^{B}\mathbf{p}_{\text{th3,4}} = [0 \;\; -0.375 \;\; \pm 0.10]\,\text{m}$
Bottom thrusters position	${}^{B}\mathbf{p}_{\text{th5,6}} = [\pm 0.40 \;\; 0 \;\; -0.125]\,\text{m}$
Damping coefficients	$K_{\text{ang}} = 4,\ K_{\text{lin}} = 2$

6.1. Vehicle model aiding

The VD aiding technique is validated using the 6-DOF rigid body model described in Section 3.1, with the parameters detailed in Table 3. The external VD, embedded VD and a classical GPS/INS architectures are studied for the rigid body model subject to constant linear and centripetal acceleration, describing the upwards trimming trajectory shown in Fig. 5(a). The bias estimation and compensation is analyzed by considering a 30% bias calibration error in each channel of the accelerometer and rate gyro sensors. A magnetometer is also integrated in the system, using the measurement residual model (25).

The linear and angular velocity information provided by the vehicle model clearly endows the filter to compensate for the inertial sensor biases, as shown in Fig. 5. Accelerometer bias calibration errors are reduced almost instantly by the VD aided navigation system, as shown in Fig. 5(b), yielding smaller bias steady-state estimation error, and allowing for smaller estimations errors of the other state variables. Fig. 5(c) evidences the same accuracy enhancements on the rate gyro bias estimation, for a VD aided navigation system without magnetometer observations. The velocity results are dramatically enhanced by the VD aiding, as shown in Fig. 5(d) and detailed

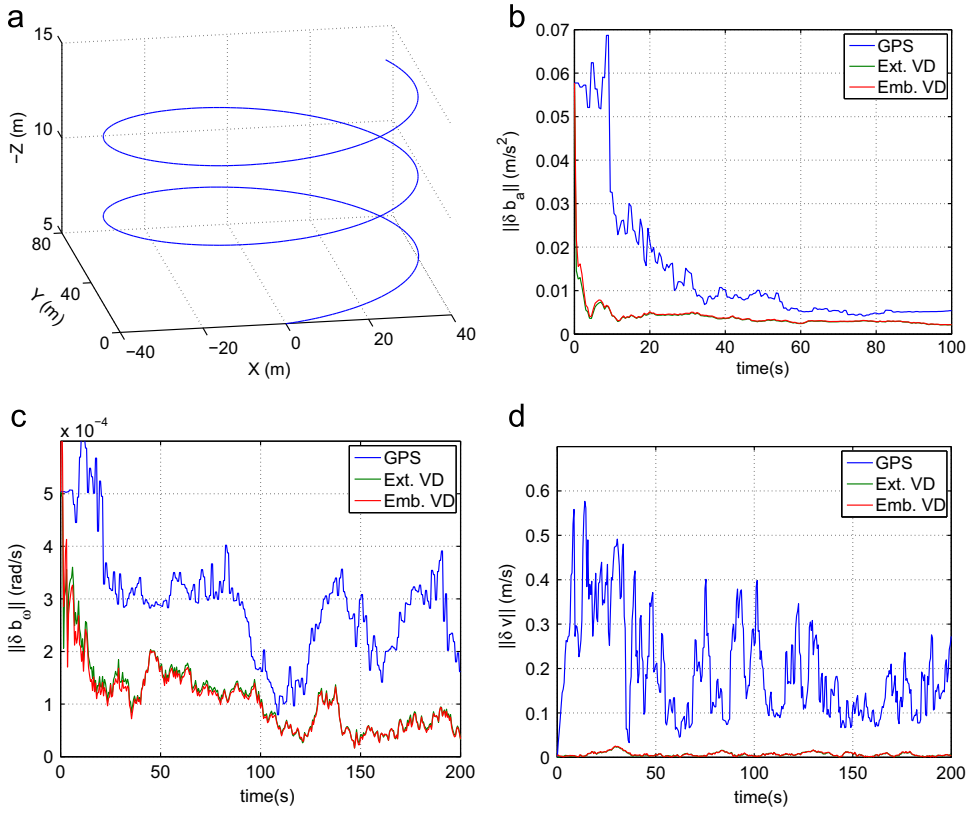

Fig. 5. Simulation results of the GPS and the VD aided navigation systems (rigid body). (a) Trimming trajectory. (b) Accelerometer bias estimation error. (c) Rate gyro bias estimation error. (d) Velocity estimation error.

Table 4
Estimation error (rigid body).

Aiding information	RMS				
	$\|\delta\mathbf{p}\|$ (m)	$\|\delta\mathbf{v}\|$ (m/s)	Yaw error (°)	Pitch error (°)	Roll error (°)
GPS	1.83	2.27×10^{-1}	1.35×10^{-2}	7.60×10^{-2}	7.59×10^{-2}
Extended VD	1.31×10^{-1}	8.00×10^{-3}	1.22×10^{-2}	1.70×10^{-2}	1.75×10^{-2}
Embedded VD	1.35×10^{-1}	8.32×10^{-3}	1.21×10^{-2}	1.71×10^{-2}	1.70×10^{-2}
Embedded VD (z_v only)	1.38×10^{-1}	7.88×10^{-3}	1.35×10^{-2}	1.70×10^{-2}	1.63×10^{-2}

Table 5
Execution time of the navigation systems for 200 s of simulation time.

	GPS aided	External VD aided	Embedded VD aided	
			$(\boldsymbol{\omega}, {}^B\mathbf{v})$ aiding	${}^B\mathbf{v}$ aiding
Execution time (s)	293	543	400	310

in Table 4. Although position and attitude information are not directly provided for by the vehicle model, position and attitude estimates are more accurate with VD aiding, as shown in Table 4, due to the smaller velocity and bias estimation errors.

The accuracy of the embedded and the external VD architectures are similar, which validates the proposed aiding technique. Both architectures use the same vehicle model, and hence the aiding information introduced in the filter is the same, and the estimation results are thus similar. However, the embedded VD aiding brings about computational savings, as demonstrated in the simulation execution times presented in Table 5. As discussed in Section 3.3, the smaller number of states associated with the embedded VD aiding, and the propagation of solely the angular velocity, reduce the computational cost of using the vehicle model information in the system.

The embedded VD aiding allows for the independent use of the angular and linear velocity aiding, as opposed to using the full dynamics computed by the external vehicle simulator. Interestingly enough, simulation runs for the embedded VD aiding using only the velocity observation, i.e. $\mathbf{z}_C = \mathbf{z}_v$, show that the execution time is close to that of the GPS aided architecture, while the estimation results, shown in Table 4, are very similar to those of the linear and angular velocity aiding case. Although the angular velocity component is a valuable contribution in general, the accuracy improvements obtained by using solely the linear velocity aiding suggest that, for some operating scenarios, merging the velocity information of the vehicle model brings about good accuracy results, at a very small computational cost.

Note that the execution times presented in Table 5 were obtained in a Matlab 7.3 implementation, running on a Pentium 4 CPU 3 GHz with a Linux operating system, and were presented for the purpose of comparing the diverse navigation systems. The computational efficiency of the implemented EKF algorithm, that is common to all of the analyzed architectures, is beyond the scope of the present work. The filter implementation can be further improved by adopting numerically efficient and/or suboptimal formulations described in Brown and Hwang (1997), Gelb (1974) and references therein. Also, the proposed VD aiding was studied using low-cost sensors, but high-end solutions can be considered. The analysis of the trade-off between sensor specifications and estimate accuracy is beyond the scope of this work, for in-depth GPS unit error characterization and budgeting techniques the reader is referred to Grewal et al. (2007) and Farrell and Barth (1999).

Fig. 6. Vario X-Treme model-scale helicopter.

6.2. Vario X-Treme helicopter

The dynamic model of the fully actuated 6-DOF rigid body was adopted to illustrate and validate the proposed aiding technique. In this section, simulation results are presented for the Vario X-Treme helicopter, depicted in Fig. 6. This autonomous helicopter features a six degrees of freedom rigid body dynamic model driven by external forces and moments that encompass the main rotor and tail rotor effects, including the first order blade pitching dynamics with Bell–Hiller mechanism and the steady-state blade flapping dynamics. The model dynamics, derived from first-principles in Cunha and Silvestre (2003) and Cunha, Guerreiro, and Silvestre (2005), are summarized in Appendix A, and research on the modeling of unmanned model-scale helicopters can be found in Mettler (2002), Kim and Tilbury (2004), and Vissière (2008) and in references therein. The considered model, although simplified, is highly nonlinear and coupled, and is adopted to take a step towards the implementation of the embedded VD aiding technique in field applications.

The simulated takeoff trajectory, depicted in Fig. 7, consists of an ascending turn, followed by a straight upwards path. A 30% bias calibration error is assumed and a magnetometer is also incorporated in the navigation system.

Although the Vario X-Treme model is highly nonlinear, the combination of the embedded VD aiding with the linear extended Kalman filtering yields accurate velocity, position, and attitude estimates, as presented in Table 6. The helicopter model aiding enhances the INS estimates, as shown in the bias and velocity errors illustrated in Fig. 8 and in the position results of Fig. 9. Bias compensation errors are effectively reduced and velocity estimation is enhanced. The position results presented in Table 6 and depicted in Fig. 9 show that the VD aiding technique effectively enhances the trajectory estimation to a sub-metric accuracy. The filter estimated error covariance is, in general, consistent with the estimation errors.

Interestingly enough, the estimation errors using only the linear velocity information of the helicopter model, shown in Table 6, are close to the results using the full information of the helicopter dynamics. This suggests that the linear velocity

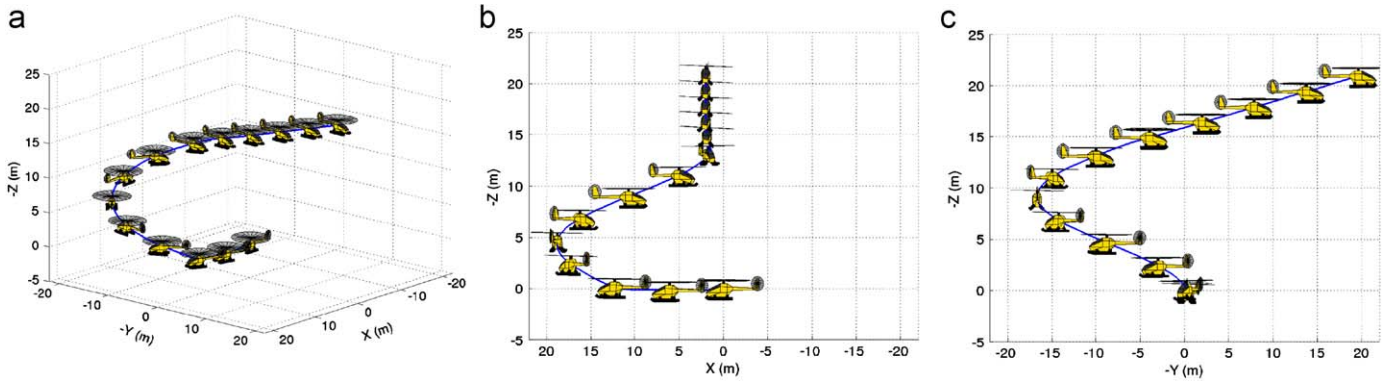

Fig. 7. Vario X-Treme simulated trajectory. (a) 3D view. (b) *xz*-plane projection. (c) *yz*-plane projection.

Table 6
Estimation error (Vario X-Treme helicopter).

Aiding information	RMS				
	$\|\delta\mathbf{p}\|$ (m)	$\|\delta\mathbf{v}\|$ (m/s)	Yaw error (°)	Pitch error (°)	Roll error (°)
GPS	2.42	3.50×10^{-1}	1.26×10^{-2}	9.15×10^{-2}	7.95×10^{-2}
Vario X-Treme model	3.07×10^{-1}	2.84×10^{-2}	1.27×10^{-2}	2.10×10^{-2}	1.31×10^{-2}
Vario X-Treme model (z_v only)	5.91×10^{-1}	3.20×10^{-2}	1.26×10^{-2}	2.17×10^{-2}	1.40×10^{-2}

information of the vehicle model can be exploited in aerial applications, requiring only the computational resources necessary to process a state observation.

As discussed in Julier and Durrant-Whyte (2003) and Koifman and Bar-Itzhack (1999), the VD aiding results must be addressed with care. Vehicle modeling errors, model simplification assumptions or unmodeled time-varying parameters and disturbances, such as vehicle load and wind gusts, may severely affect the navigation system performance if not correctly accounted for in the filter. The tuning of the noise covariance matrices, the estimation of additional states and parameters and the use of more accurate vehicle model dynamics, among other techniques (Julier & Durrant-Whyte, 2003), are adopted to allow for the use of VD in real navigation systems. Nonetheless, side effects such as the poor observability of the augmented states, the over-parametrization of the vehicle model or even the inability to model the real vehicle dynamics may occur.

Encouraging experimental results have been recently reported in Vissière et al. (2008) for a Vario Benzin Acrobatic model-scale helicopter, and in Hegrenaes et al. (2008) for the HUGIN 4500 underwater vehicle. Also, exploiting simple vehicle motion constraints yields noticeable accuracy improvements in the experimental results presented in Dissanayake and Sukkarieh (2001) for a land vehicle. Vehicle model aiding is also suitable for indoor missions where the vehicle model is known, and aiding information may be limited. The practical results evidence that either full, or simplified, vehicle models can effectively enhance the estimation results of GPS/INS architectures. The integration of the vehicle dynamics in the navigation system is a valuable aiding technique, for applications where other external sensors are not available or provide poor observability of the vehicle states.

6.3. LASER aiding

The LASER range sensor implementation is analyzed for a landing operation of an air vehicle equipped with a standard GPS/INS unit. The vehicle hovers the landing zone, as illustrated in Fig. 4, and activates the LASER at $t = 20\,\text{s}$ to acquire an accurate distance-to-ground estimate. The terrain height is $h_S = 4\,\text{m}$, the LASER is oriented along the z-axis of the body frame, that is ${}^{B}_{M}\mathbf{R} = \mathbf{I}$, and the sensor noise is characterized in Table 2.

The estimation results depicted in Fig. 10 show that the LASER sensor brings about accurate position and velocity estimates on the z-axis, whereas using solely the GPS sensor yields high uncertainty on the position estimate, which may render landing unfeasible. The velocity and distance-to-ground estimation errors, illustrated in Figs. 10(b) and (c), respectively, are reduced almost instantly when the LASER is activated. Assuming that the initial terrain height h_S uncertainty is 0.1 m, the position estimate is also enhanced, as shown in Fig. 10(a). If the uncertainty about the terrain height is larger, then the position estimate error will converge slower to smaller values, as illustrated in Fig. 11(a) for an initial h_S uncertainty of 1 m. Nonetheless, the distance to ground is acquired immediately, as shown in Fig. 11(c).

This behavior is justified by noting that p_z is related to h_S and h_V by (16), and that accurate LASER range measurements bring about precise h_V estimates. If little is known about h_S, then (16) implies that the uncertainty of h_S and of p_z are identical, and the filter can reduce the uncertainty on p_z only by using the model (15), that is a low frequency process, and hence $\hat{h}_S$ and $\hat{p}_z$ will converge slowly in time. Conversely, if h_S is known accurately, then (16) implies that p_z can be inferred accurately, as shown in Fig. 10(a).

As expected, the velocity and distance-to-ground estimate enhancements are independent of the available terrain height information, as seen by comparing Figs. 10(b) and (c) with Figs. 11(b) and (c), respectively. These results show that the LASER range finder is critical for landing the robotic platform safely, by allowing for accurate distance-to-ground and vehicle velocity estimates. Position and ground height estimation is also enhanced in the medium term, by combining LASER and GPS measurements.

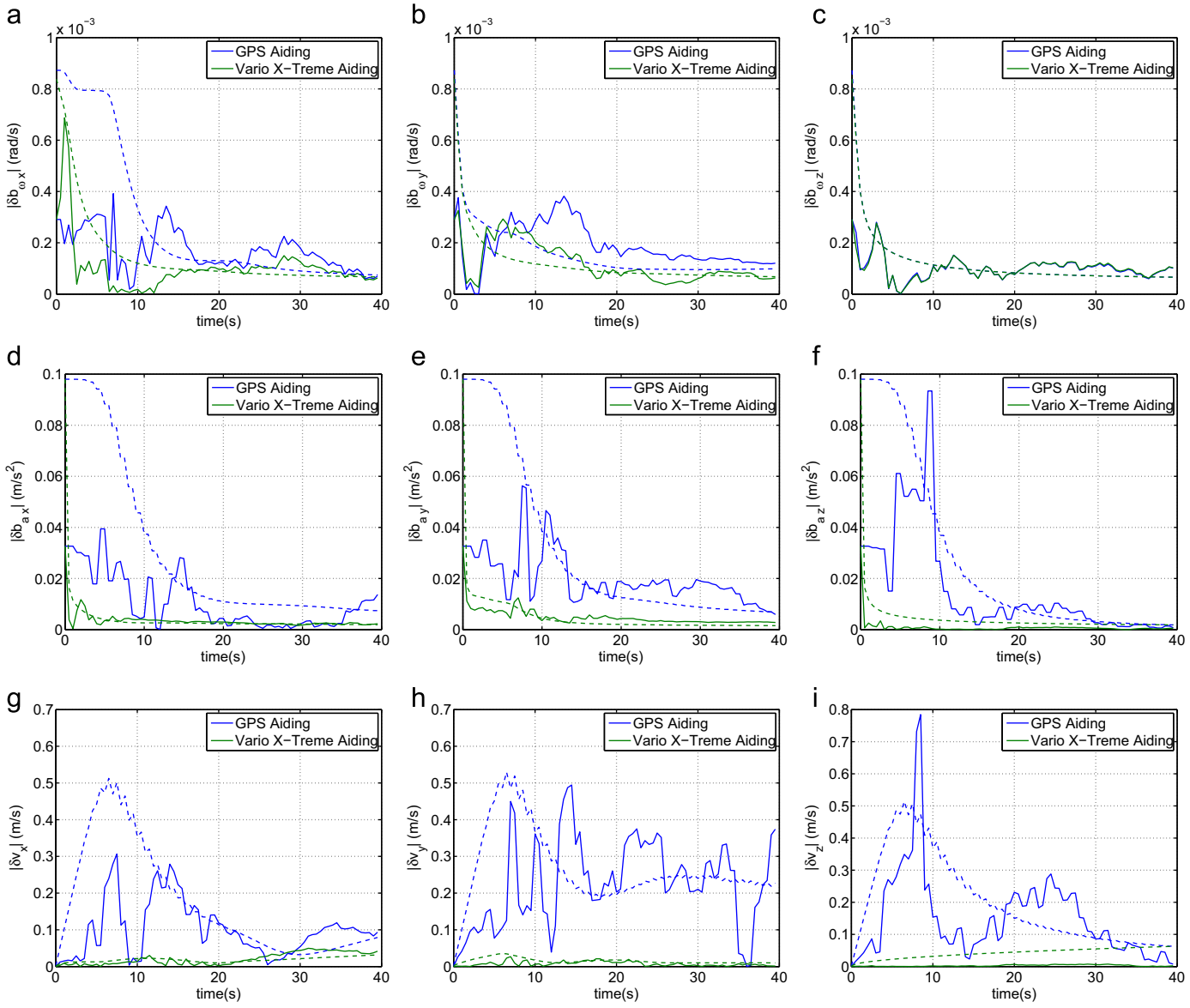

Fig. 8. Vario X-Treme VD vs GPS aiding estimation errors (solid line) and estimated error standard deviation (dashed line). (a,b,c) Rate gyro bias. (d,e,f) Accelerometer bias. (g,h,i) Velocity.

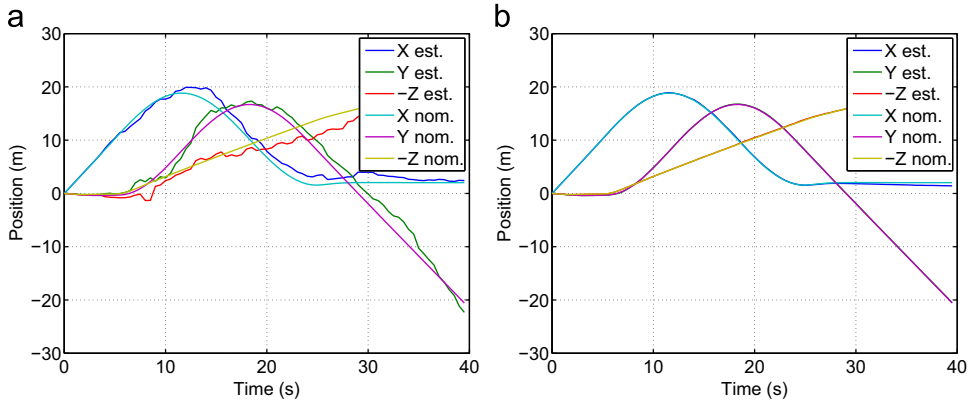

Fig. 9. Trajectory estimation for the Vario X-Treme. (a) GPS aiding. (b) Vario X-Treme model aiding.

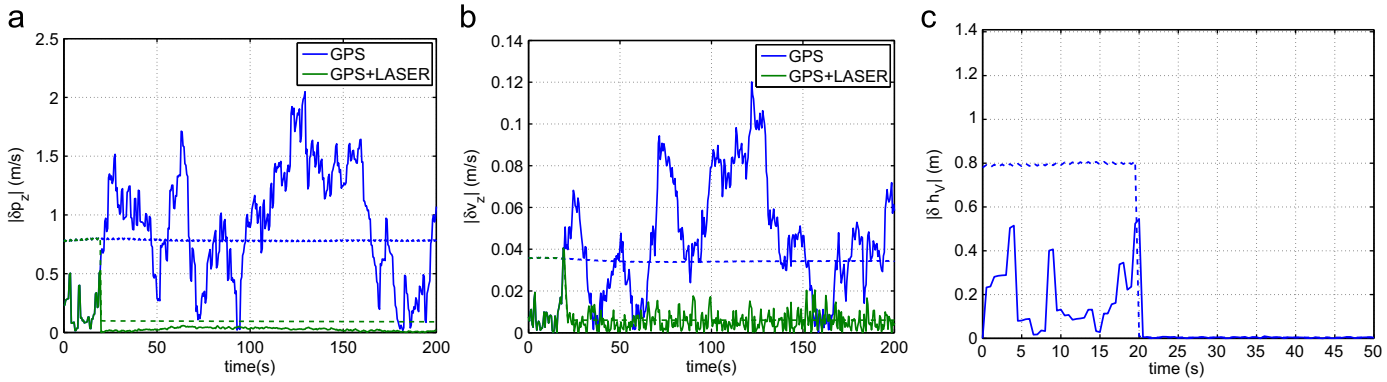

Fig. 10. LASER aiding estimation errors (solid line) and estimated error standard deviation (dashed line). (a) z-axis position (p_z). (b) z-axis velocity (v_z). (c) Vehicle height (h_V).

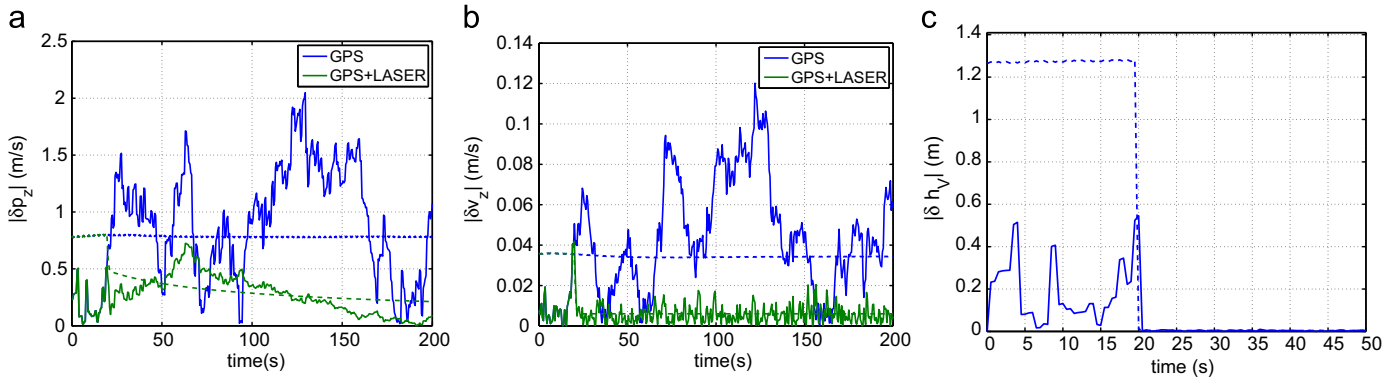

Fig. 11. LASER aiding estimation errors (solid line) and estimated error standard deviation (dashed line), large initial terrain height uncertainty. (a) z-axis position (p_z). (b) z-axis velocity (v_z). (c) Vehicle height (h_V).

7. Conclusion

A new embedded methodology to integrate the vehicle dynamics in the navigation system was proposed. The embedded VD system accuracy was shown to be equivalent that of the classical external vehicle model architecture, but with smaller computational cost and with a flexible choice of vehicle model differential equations. The application of the proposed technique to a highly nonlinear Vario X-Treme helicopter model validated the approach for realistic uninhabited air vehicles.

Trimming trajectory simulation results showed that the bias calibration errors were quickly compensated and that long-term bias estimates were enhanced. The linear and angular velocity were improved with respect to the classical GPS/INS configuration. Position and attitude errors, although not directly observable by the VD model, were improved due to the enhancements in velocity estimation.

The proposed methodology allows for the decoupling of the vehicle model differential equations. In particular, the linear velocity information of the VD model was exploited directly in the filter in the form of a measurement residual, and the associated computational cost was only that of computing the measurement matrix and the Kalman gain. Given the exciting accuracy enhancements obtained using solely the linear velocity model, and the small computational cost of the implementation, this aiding information steps forward as an exciting, software based technique, suitable for most practical applications even with computational constraints.

Finally, the LASER range finder sensor provided high precision distance-to-ground estimates for takeoff and landing maneuvers. It was shown that integrating the sensor produced accurate vehicle height and vertical velocity estimates, suitable for safe maneuvering of the autonomous vehicle. It was shown that the estimate of the vehicle position with respect to Earth frame is also improved, according to the uncertainty on the terrain height.

The computational flexibility and savings introduced by the embedded VD aiding motivate the experimental validation of the navigation system on a Vario X-Treme model-scale helicopter. While the model of the Vario X-Treme has been derived in Cunha and Silvestre (2003), the problem of model uncertainty, aerodynamic coefficient determination, structural vibration and flexibility, disturbances in the vehicle inputs, time-delay in the actuation, among others, must be accounted for. The implementation of the proposed VD aiding technique in aerial vehicles is strongly encouraged by the experimental results obtained in Vissière et al. (2008) and Hegrenaes et al. (2008), by the study of non-ideal VD model aiding presented in Julier and Durrant-Whyte (2003) and Koifman and Bar-Itzhack (1999), and by the fact that VD linear velocity yields significant accuracy enhancements as shown in Section 6 and may be simply exploited using a measurement residual.

Acknowledgements

This work was partially supported by Fundação para a Ciência e a Tecnologia (ISR/IST plurianual funding) through the POS_Conhecimento Program that includes FEDER funds and by the PTDC/EEA-ACR/72853/2006 HELICIM project. The work of J.F. Vasconcelos and B. Guerreiro was supported by the PhD Student Scholarships SFRH/BD/18954/2004 and SFRH/BD/21781/2005, respectively, from the Portuguese FCT POCTI programme.

Appendix A. Helicopter model summary

This section briefly describes the nonlinear Vario X-Treme helicopter model presented in Cunha and Silvestre (2003), deduced from first principles, and simplified under the assumptions described in Cunha et al. (2005), for further references on small-scale helicopters modeling see Mettler (2002), Kim and Tilbury (2004) and references therein. As the complete model, the simplified model considers a six degrees of freedom rigid body dynamics driven by the external forces and moments generated by the several components of helicopter, however, the contributions of the fuselage, horizontal tailplane and vertical tail fin are considered to be negligible. This model also considers simplified versions of the first order dynamics for the main rotor blade pitch motion with Bell-Hiller mechanism, the steady state dynamics for the main rotor blade flap dynamics and the blade lag dynamics are neglected.

The motion of the helicopter is described using the rigid body equations of motion

$$\dot{\boldsymbol{\omega}} = \mathbf{I}_B^{-1}(\mathbf{n}(\boldsymbol{\omega}, {}^B\mathbf{v}, \mathbf{u}_{hc}) - \boldsymbol{\omega} \times \mathbf{I}_B\boldsymbol{\omega}),$$

$${}^B\dot{\mathbf{v}} = -\boldsymbol{\omega} \times {}^B\mathbf{v} + \frac{1}{m}\mathbf{f}(\boldsymbol{\omega}, {}^B\mathbf{v}, \mathbf{u}_{hc}) + \mathcal{R}'^E\mathbf{g}, \quad \dot{\mathcal{R}} = \mathcal{R}(\boldsymbol{\omega})_\times,$$

where m is the vehicle mass, $\mathbf{I}_B$ is the tensor of inertia about the Center of Mass coordinate frame, denoted by $\{G\}$, $\mathbf{u}_{hc}$ is the helicopter command vector and $\mathbf{f}$ and $\mathbf{n}$ are the vectors of external forces and moments, respectively, along the same frame. The input vector $\mathbf{u}_{hc} = [\theta_{c_0}\ \theta_{c_{1c}}\ \theta_{c_{1s}}\ \theta_{c_{0_t}}]'$ comprises the blade pitch angle commands for the main rotor collective θ_{c_0}, main rotor longitudinal cyclic $\theta_{c_{1c}}$, main rotor lateral cyclic $\theta_{c_{1s}}$ and the tail rotor collective $\theta_{c_{0_t}}$. To model the non-symmetric shape of the rotor blades, θ_{c_0} and $\theta_{c_{0_t}}$ swashplate inputs are corrected in the helicopter model using the variables $\theta_0 = \theta_{c_0} + \alpha_0$ and $\theta_{0_t} = \theta_{c_{0_t}} + \alpha_{0_t}$, where α_0 and α_{0_t} are the lift curve slope offsets for the main and tail rotor blades, respectively.

As noted before, for smooth low velocity maneuvers, the effects of the fuselage, horizontal tailplane and vertical fin on the overall dynamics are negligible. For this reason, the total force and moment vectors are modeled accounting only for the two most dominant components of a helicopter, the main rotor and the tail rotor, yielding $\mathbf{f} = \mathbf{f}_{mr} + \mathbf{f}_{tr}$, $\mathbf{n} = \mathbf{n}_{mr} + \mathbf{n}_{tr}$, where the subscripts mr and tr stand, respectively, for the main rotor and tail rotor components. The main rotor is the primary source of lift, required to sustain the helicopter, and generates other forces and moments that allow for the control of position, orientation and velocity of the helicopter. The main rotor forces and moments are described by

$$\mathbf{f}_{mr} := \begin{bmatrix} X_{mr} \\ Y_{mr} \\ Z_{mr} \end{bmatrix} = -s_1 \begin{bmatrix} a_0\left(\frac{1}{2}\theta_{1s}\lambda_0 + \mu\lambda_0\theta_0\right) + \delta_0\mu \\ a_0\left(\frac{1}{2}\theta_{1c}\lambda_0\right) \\ a_0\left(\frac{2}{3}\theta_0 - \lambda_0\right) \end{bmatrix},$$

$$\mathbf{n}_{mr} = \begin{bmatrix} -k_\beta\beta_{1s} + Y_{mr}h_R \\ -k_\beta\beta_{1c} - X_{mr}h_R + Z_{mr}x_{cm} \\ \frac{1}{2}s_2\delta_0 + s_2a_0\left(\frac{2}{3}\theta_0\lambda_0 - \lambda_0^2\right) - Y_{mr}x_{cm} \end{bmatrix},$$

where s_1 and s_2 are the main rotor's force and moment normalizing constants, a_0 is the lift curve slope, δ_0 is the profile drag coefficient, k_β is the center-spring rotor stiffness, and x_{cm} and h_R determine the position of the main rotor hub aft and above the center of mass, respectively. The remaining undefined variables are defined hereafter.

In helicopters equipped with the Bell-Hiller mechanism (Cunha & Silvestre, 2003), the cyclic blade pitch angles result from the combination of the commands introduced by the swashplate and the flybar flapping motion. The simplified first order blade pitch dynamics of the main rotor are described by

$$\dot{\theta}_{1c} = C_{\theta_1}\theta_{1c} + C_{\theta_3}\theta_{c_{1c}}, \quad \dot{\theta}_{1s} = C_{\theta_1}\theta_{1s} + C_{\theta_3}\theta_{c_{1s}} + C_{\theta_8}\mu\lambda_0,$$

with the coefficients given by

$$C_{\theta_1} = -\frac{\Omega\gamma_f}{4\left[\left(\frac{\gamma_f}{8}\right)^2 + 4\right]}, \quad C_{\theta_3} = \frac{\Omega(c_4 + c_1)\gamma_f}{4c_2\left[\left(\frac{\gamma_f}{8}\right)^2 + 4\right]}, \quad C_{\theta_8} = -\frac{\eta_2\Omega\gamma_f}{2c_2\left[\left(\frac{\gamma_f}{8}\right)^2 + 4\right]},$$

where μ stands for the normalized forward velocity at the main rotor, λ_0 is the normalized collective downwash induced by main rotor, Ω is the main rotor angular speed, γ_f is the flybar lock number, and c_1, c_2 and c_4 are flybar pitching parameters.

The main rotor blade flapping motion is described by the blade flap angle vector $\boldsymbol{\beta} = [\beta_0\ \beta_{1c}\ \beta_{1s}]$, where β_0 denotes the collective mode, and β_{1c} and β_{1s} represent the longitudinal and lateral cyclic modes, respectively. The blade flapping dynamics of the main rotor can be approximated by the simplified steady-state solution given by

$$\beta_0 = C_{\beta_1}\theta_0, \quad \beta_{1c} = C_{\beta_3}\mu\theta_0 + C_{\beta_4}\theta_{1c} - C_{\beta_5}\theta_{1s} + C_{\beta_6}\omega_x + C_{\beta_7}\omega_y + C_{\beta_8}\mu\lambda_0 - C_{\beta_4}\lambda_{1c},$$

$$\beta_{1s} = C_{\beta_9}\mu\theta_0 + C_{\beta_5}\theta_{1c} + C_{\beta_4}\theta_{1s} + C_{\beta_7}\omega_x - C_{\beta_6}\omega_y + C_{\beta_{10}}\mu\lambda_0 - C_{\beta_5}\lambda_{1c},$$

with the state coefficients

$$C_{\beta_1} = \frac{\frac{\gamma}{8}}{\frac{\gamma}{8}S_\beta + 1}, \quad C_{\beta_3} = -\frac{\frac{8}{3}}{S_\beta^2 + 1}, \quad C_{\beta_4} = \frac{S_\beta}{S_\beta^2 + 1}, \quad C_{\beta_5} = \frac{1}{S_\beta^2 + 1},$$

$$C_{\beta_6} = \frac{16}{\Omega\gamma}\frac{S_\beta}{S_\beta^2 + 1}, \quad C_{\beta_7} = \frac{16}{\Omega\gamma}\frac{1}{S_\beta^2 + 1}, \quad C_{\beta_8} = \frac{2}{S_\beta^2 + 1},$$

$$C_{\beta_9} = \frac{\frac{8}{3}S_\beta}{S_\beta^2 + 1}, \quad C_{\beta_{10}} = -\frac{2S_\beta}{S_\beta^2 + 1},$$

where S_β is the blade stiffness number, R_m is the main rotor radius and γ is the lock number.

The tail rotor, placed at the tail boom in order to counteract the moment generated by the rotation of the main rotor, provides yaw control of the helicopter. Following the same principles used for the main rotor and neglecting blade pitch, flap and lag dynamics, the simplified expressions for the tail rotor force and torque are given by

$$\mathbf{f}_{tr} := \begin{bmatrix} X_{tr} \\ Y_{tr} \\ Z_{tr} \end{bmatrix} = s_{1_t}a_{0_t}\begin{bmatrix} 0 \\ \frac{2}{3}\theta_{0_t} - \lambda_{0_t} \\ 0 \end{bmatrix}, \quad \mathbf{n}_{tr} = \begin{bmatrix} Y_{tr}h_{tr} \\ -\frac{1}{2}s_{2_t}\delta_{0_t} - s_{2_t}a_{0_t}\left(\frac{2}{3}\theta_{0_t}\lambda_{0_t} - \lambda_{0_t}^2\right) \\ -Y_{tr}(x_{cm} + l_{tr}) \end{bmatrix},$$

where λ_{0_t} is the collective induced downwash of the tail rotor, s_{1_t} and s_{2_t} are the tail rotor's force and moment normalizing constants, a_{0_t} is the tail rotor lift curve slope, δ_{0_t} is the tail rotor profile drag coefficient, l_{tr} is the distance from the tail rotor hub to the fuselage reference point and h_{tr} is the height of tail rotor hub above the fuselage reference point.

The induced downwash results from the thrust force generated at the surface of the rotating blades that accelerates the air downwards creating a flowfield. By decomposing the downwash in Fourier series and neglecting the second and higher order terms, results in the collective, longitudinal and lateral cyclic components, respectively, λ_0, λ_{1c} and λ_{1s}. The collective components of the induced downwash at the main and tail rotors are given by

$$\lambda_0 = -\frac{a_0 s}{16} + \sqrt{\left(\frac{a_0 s}{16}\right)^2 + \frac{a_0 s}{12}\theta_0}, \quad \lambda_{0_t} = -\frac{a_{0_t} s_t}{16} + \sqrt{\left(\frac{a_{0_t} s_t}{16}\right)^2 + \frac{a_{0_t} s_t}{12}\theta_{0_t}},$$

where s and s_t are the solidity constants of the main and tail rotors, respectively. Finally, the main rotor longitudinal cyclic

induced downwash and the forward normalized velocity are described by

$$\lambda_{1c} = \begin{cases} 0 & \text{if } \mu = 0 \text{ (vertical flight)}, \\ \lambda_0 \left(\sqrt{1 + \left(\frac{\lambda_0}{\mu}\right)^2} - \left|\frac{\lambda_0}{\mu}\right| \right) & \text{otherwise}, \end{cases} \qquad \mu = \frac{u_x - h_R \omega_y}{\Omega R_m},$$

whereas the main rotor lateral cyclic downwash is neglected $\lambda_{1s} = 0$ as well as both tail rotor cyclic downwash components.

References

Bar-Shalom, Y., Li, X. R., & Kirubarajan, T. (2001). *Estimation with applications to tracking and navigation*. Wiley-Interscience.

Bijker, J., & Steyn, W. (2008). Kalman filter configurations for a low-cost loosely integrated inertial navigation system on an airship. *Control Engineering Practice*, *16*(12), 1509–1518.

Britting, K. R. (1971). *Inertial navigation systems analysis*. New York: Wiley, Inc.

Brown, R., & Hwang, P. Y.C. (1997). *Introduction to random signals and applied Kalman filtering* (3rd ed.). New York: Wiley, Inc.

Bryson, M., & Sukkarieh, S. (2004). Vehicle model aided inertial navigation for a UAV using low-cost sensors. In *Australasian conference on robotics and automation*, Canberra, Australia, December.

Craig, J. (1989). *Introduction to robotics* (2nd ed.). New York: Addison-Wesley.

Cunha, R., Guerreiro, B., & Silvestre, C. (2005). Vario X-treme helicopter nonlinear model: Complete and simplified expressions. Technical Report, Institute for Systems and Robotics.

Cunha, R., & Silvestre, C. (2003). Dynamic modeling and stability analysis of model-scale helicopters with Bell-Hiller stabilizing bar. *AIAA guidance, navigation and control conference*.

Dissanayake, G., & Sukkarieh, S. (2001). The aiding of a low-cost strapdown inertial measurement unit using vehicle model constraints for land vehicle applications. *IEEE Transactions on Robotics and Automation*, *17*(5), 731–747.

Farrell, J., & Barth, M. (1999). *The global positioning system and inertial navigation*. New York: McGraw-Hill.

Gelb, A. (1974). *Applied optimal estimation*. Cambridge, MA: MIT Press.

Goshen-Meskin, D., & Bar-Itzhack, I. Y. (1992a). Observability analysis of piece-wise constant systems—part i: Theory. *IEEE Transactions on Aerospace and Electronic Systems*, *28*(4), 1056–1067.

Goshen-Meskin, D., & Bar-Itzhack, I. Y. (1992b). Observability analysis of piece-wise constant systems—part ii: Application to inertial navigation in-flight alignment. *IEEE Transactions on Aerospace and Electronic Systems*, *28*(4), 1068–1075.

Grewal, M. S., Weill, L. R., & Andrews, A. P. (2007). *Global positioning systems, inertial navigation, and integration* (2nd ed.). Wiley-Interscience.

Guerreiro, B., Silvestre, C., Oliveira, P., & Vasconcelos, J. F. (2008). Nonlinear and geometric optimization methods for LADAR calibration. In *IEEE international conference on robotics and automation* (pp. 1406–1411).

Hegrenaes, O., Berglund, E., & Hallingstad, O. (2008). Model-aided inertial navigation for underwater vehicles. In *IEEE international conference on robotics and automation* (pp. 1069–1076).

Ignagni, M. B. (1998). Duality of optimal strapdown sculling and coning compensation algorithms. *Journal of the Institute of Navigation*, *45*(2), 85–95.

Julier, S., & Durrant-Whyte, H. F. (2003). On the role of process models in autonomous land vehicle navigation systems. *IEEE Transactions on Robotics and Automation*, *19*(1), 1–13.

Kim, S. K., & Tilbury, D. M. (2004). Mathematical modeling and experimental identification of an unmanned helicopter robot with flybar dynamics. *Journal of Robotic Systems*, *21*(3), 95–116.

Koifman, M., & Bar-Itzhack, I. Y. (July 1999). Inertial navigation system aided by aircraft dynamics. *IEEE Transactions on Control Systems Technology*, *7*(4), 487–493.

Lefferts, E. J., Markley, F. L., & Shuster, M. D. (1982). Kalman filtering for spacecraft attitude estimation. *Journal of Guidance, Control, and Dynamics*, *5*(5), 417–429.

Ma, X., Sukkarieh, S., & Kim, J. (2003). Vehicle model aided inertial navigation. In *IEEE intelligent transportation systems* (Vol. 2, pp. 1004–1009), Shangai, China.

Markley, F. L. (2003). Attitude error representations for Kalman filtering. *AIAA Journal of Guidance, Control, and Dynamics*, *26*(2), 311–317.

Mettler, B. (2002). *Identification modeling and characteristics of miniature rotorcraft*. New York: Springer.

Morgado, M., Oliveira, P., Silvestre, C., & Vasconcelos, J. F. (2007). Vehicle dynamics aiding technique for USBL/INS underwater navigation system. In *IFAC conference on control applications in marine systems*, Bol, Croatia.

Pflimlin, J.-M., Binetti, P., Souères, P., Hamel, T., & Trouchet, D. (2009). Modeling and attitude control analysis of a ducted-fan micro aerial vehicle. *Control Engineering Practice*, in press, doi:10.1016/j.conengprac.2009.09.009.

Pittelkau, M. (2003). Rotation vector in attitude estimation. *AIAA Journal of Guidance, Control, and Dynamics*, *26*(6), 855–860.

Rogers, R. M. (2003). Applied mathematics in integrated navigation systems. AIAA.

Salazar-Cruz, S., Lozano, R., & Escareño, J. (2009). Stabilization and nonlinear control for a novel trirotor mini-aircraft. *Control Engineering Practice*, *17*(8), 886–894.

Savage, P. (1998a). Strapdown inertial navigation integration algorithm design part 1: Attitude algorithms. *AIAA Journal of Guidance, Control, and Dynamics*, *21*(1), 19–28.

Savage, P. (1998b). Strapdown inertial navigation integration algorithm design part 2: Velocity and position algorithms. *AIAA Journal of Guidance, Control, and Dynamics*, *21*(2), 208–221.

Vasconcelos, J. F., Oliveira, P., & Silvestre, C. (2005). Inertial navigation system aided by GPS and selective frequency contents of vector measurements. In *AIAA guidance, navigation, and control conference*, San Francisco, USA.

Vasconcelos, J. F., Silvestre, C., & Oliveira, P. (2006). Embedded vehicle dynamics and LASER aiding techniques for inertial navigation systems. In *AIAA guidance, navigation, and control conference*, Keystone, CO, USA.

Vissière, D. (2008). Guidance navigation and control solutions for unmanned heterogeneous vehicles during a collaborative mission. Ph.D. thesis, CAS-Centre automatique et systèmes.

Vissière, D., Bristeau, P.-J., Martin, A. P., & Petit, N. (2008). Experimental autonomous flight of a small-scaled helicopter using accurate dynamics model and low-cost sensors. In *17th IFAC World Congress*.